

GEOCHEMICAL INVESTIGATION
OF ROSITA HILLS VOLCANIC COMPLEX,
CUSTER COUNTY, COLORADO

by

Joseph Smalley

B.S., Wright State University, 1977

A MASTER'S THESIS

submitted in partial fulfillment of the
requirements for the degree

MASTER OF SCIENCE

Department of Geology
KANSAS STATE UNIVERSITY
Manhattan, Kansas

1981

Approved by


Major Professor

SPEC
COLL
LD
2668
.T4
1981
565
c. 2

A11200 093397

CONTENTS

INTRODUCTION	1
Previous investigations	2
Petrology of the Rosita Hills volcanic district . . .	4
Pre-volcanic rocks	4
Rhyolitic pyroclastic rocks	4
Rosita Formation	5
Hornblende trachyandesite	5
Rhyodacite	6
Rhyolite	6
Bunker Hill Trachyandesite	7
Syenodiorite	7
Latite	7
Trachyte	8
Lamprophyre	8
Geochronology	9
EXPERIMENTAL METHODS	12
Sample collection and preparation	12
Atomic absorption and flame emission spectrophotometry	13
Sample dissolution procedure	13
Sample dilutions	13
Standard solutions	14
Analytical precision	14
Instrumental neutron-activation analysis	18
Instrumentation	18
Procedure	18
Calculations	19
Analytical precision	20
Mass Spectrometry	22
Sample preparation	22
Sample analysis	22
X-ray fluorescence	24

CONTENTS

RESULTS	25
Major elements	25
Trace elements	35
Rare earth elements	39
Strontium isotope ratios	44
Petrography	45
DISCUSSION	49
Evidence of fractional crystallization	49
Theories concerning the origin of alkali-calcic magmas	53
Trace-element modeling	57
Modeling of fractional crystallization trends	59
Relationship between rhyodacite (Tbm) and rhyolite (Trr)	61
Relationship between trachyandesite (Tb) and latite (Tp)	63
Relationship of trachyte (Tt) to other rock units	64
Relationship between syenodiorite (Tbs) and trachyandesite (Tb)	65
Relationship between syenodiorite (Tbs) and lam- prophyre (Tl)	66
Modeling of possible source materials	67
Mechanisms of magma generation	74
Comparisons to nearby igneous suites of similar geologic age	74
Conclusions	81
REFERENCES	83
APPENDICES	90
I. Petrographic descriptions	90
II. Geochemical data	103
III. Trace-element modeling equations and partition coefficients	110

LIST OF FIGURES

Figure

1	Map showing location of Rosita Hills district .	3
2	Geologic map of Rosita Hills volcanic complex .	11
3	Variation in SiO_2 concentrations (weight percent oxide) with respect to the differentiation index (D.I. = normative Q + or + ab + ne) among samples of the Rosita Hills volcanic rock suite	26
4	Variations in K_2O and Na_2O concentrations among samples of the Rosita Hills volcanic rock suite with respect to SiO_2 contents . .	28
5	Variation in Fe_2O_3 (representing total Fe content), CaO , and MgO concentrations among samples of the Rosita Hills volcanic rock suite with respect to SiO_2 contents	29
6	Alkali-iron-magnesium triangular variation diagram of samples from the Rosita Hills volcanic rock suite	31
7	Na_2O - K_2O - CaO triangular variation diagram of samples from the Rosita Hills volcanic rock suite	32
8	Alkali-lime index plot of the Rosita Hills volcanic rock suite	34
9	Variation in Sr and Rb concentrations (ppm) among samples of the Rosita Hills volcanic suite with respect to SiO_2 contents (weight-percent oxides)	36
10	Variations in the K/Rb ratio among samples of the Rosita Hills volcanic rock suite with respect to K_2O concentrations (weight-percent oxides)	37

LIST OF FIGURES

Figure

11	Variation in Sc, Ba, and Th concentrations (ppm) among samples with respect to SiO ₂ contents (weight percent oxides)	38
12a	Chondrite-normalized REE distributions of syenodiorite and lamprophyre samples	40
12b	Chondrite-normalized REE distributions of trachyandesite samples	41
12c	Chondrite-normalized REE distributions of latite and rhyodacite samples	42
12d	Chondrite-normalized REE distributions of trachyte and rhyolite samples	43
13	Predicted range of REE concentrations produced by 1 to 30 percent melting of an eclogite source with initial mineral ratio of clinopyroxene/garnet = .85/.15 which melts in a ratio of clinopyroxene/garnet = .75/.25	68
14	Predicted range of REE concentrations produced by 1 to 30 percent melting of an eclogite source with an initial mineral ratio of clinopyroxene/garnet = .95/.05 which melts in a ratio of clinopyroxene/garnet = .75/.25	69
15	Predicted range of REE concentrations in magma produced by 3 to 10 percent melting of a peridotite with an initial mineral ratio of olivine/clinopyroxene/orthopyroxene/garnet = .60/.13/.25/.02 melting in a ratio of .42/.30/.18/.10 (after Cullers and Arnold, 1980)	72
16	Partition coefficients used in trace-element modeling of basaltic magma	113
17	Partition coefficients used in trace-element modeling of silica-rich magma	115

LIST OF TABLES

Table

1	Radiometric age determinations of volcanic rock samples from the Rosita Hills district (Scott and Taylor, 1975)	9
2	Sample solutions used in atomic absorption and flame-emission analyses	15
3	Standard solutions used in atomic absorption and flame-emission analyses	16
4	Comparison of analyses of U.S.G.S. standard rocks in this study with values of Flanagan (1976)	17
5	Trace-element concentrations (ppm) in U.S.G.S. standard BCR-1 as determined by neutron activation in this study compared to analyses of others	21
6	Instrument setting and Compton scattering peaks utilized in Rb and Sr determinations by X-ray fluorescence	24
7	Sr isotope data for samples from the Rosita Hills suite	44
8	Petrographic summary of rock samples analyzed in this study	46
9	Changes in concentrations of trace elements in magma due to extraction of various mineral phases	60
10	Comparison of REE concentrations (ppm) in model sources with typical REE concentrations in basalt and peridotite	70
11	Comparison of major element concentrations in Rosita Hills samples with analyses of rocks from nearby igneous suites of similar age	75
12	Comparison of REE concentrations in Rosita Hills samples with analyses of rocks from nearby igneous suites of similar age	77

LIST OF TABLES

Table

13	Major-element analyses (weight percent oxides) and C.I.P.W. normative compositions of samples examined in this study . .	104
14	Major-element analyses of Rosita Hills samples provided by Cross (1896)	106
15	Concentrations of trace-elements in Rosita Hills samples as determined by neutron-activation analysis	107
16	Sr and Rb concentrations (ppm) of Rosita Hills samples as determined by X-ray fluorescence	109
17	Partition coefficients used in trace-element modeling of basaltic magma (compiled by Arth and Hanson, 1975)	112
18	Partition coefficients used in trace-element modeling of silica-rich magma (compiled by Arth and Hanson, 1975)	114

**THIS BOOK
CONTAINS
NUMEROUS PAGES
WITH THE ORIGINAL
PRINTING BEING
SKEWED
DIFFERENTLY FROM
THE TOP OF THE
PAGE TO THE
BOTTOM.**

**THIS IS AS RECEIVED
FROM THE
CUSTOMER.**

INTRODUCTION

The southern Colorado silver mining district known as the Rosita Hills represents the eroded remnants of an Oligocene to Miocene age andesitic volcano. The district is located about 5 miles southeast of Westcliffe, Colorado, and approximately 50 miles southwest of Colorado Springs along the eastern edge of the Wet Mountain Valley (Figure 1). Radiometric age determinations indicate that the volcanic activity of the district occurred over a period of about 6 million years and ceased approximately 25 million years ago (Scott and Taylor, 1975).

The volcanic rock units of the district consist of nearly equal volumes of trachyandesite, latite, rhyodacite, trachyte, and rhyolite with smaller volumes of syenodiorite and lamprophyre. Compositional similarities among the rock units have led previous investigators (Cross, 1896; Siems, 1967) to conclude that the different magma types extruded were derived from a common parent magma. Siems (1968) suggested that a trachyandesitic parent magma might have been formed by fusion of lower crustal material. These conclusions were based primarily on petrographic evidence and field relations together with a limited amount of chemical data provided by Cross (1896).

This investigation of the Rosita Hills Volcano focuses on the chemical characteristics of the rock units with the objective of refining the previously proposed models concerning the origin and evolution of the various magma types extruded. New geochemical data, including major element and trace element concentrations and strontium isotope ratios from representative

rock units of the district, are provided. The genetic implications of these data are then discussed in light of recent developments in the field of experimental petrology.

Previous Investigations

Silver and gold prospecting thrived within the Rosita Hills district from about 1860 to 1885, and several deep mine shafts were dug into the volcanic deposits. Several mine reports described the general nature of the rocks encountered in these mines (Wulsten, 1876; Clark, 1879; Grabil, 1883). Emmons (1896) and Cross (1896) examined the ore deposits and geological relationships among the major rock units of the province. Major element analyses were included in their reports (Appendix II).

Recent investigations of the field relationships of the province were conducted by Siems (1967, 1968) and Sharp (1978). Some aspects of their interpretations are discussed in the petrology section of this report. Kleinkopf et al. (1979) utilized gravity, seismic refraction, and aeromagnetic data in their interpretation of the subsurface geology and fault tectonics of the district. Regional studies of the petrology and structure of the adjacent Wet Mountains were conducted by Scott and Taylor (1975).

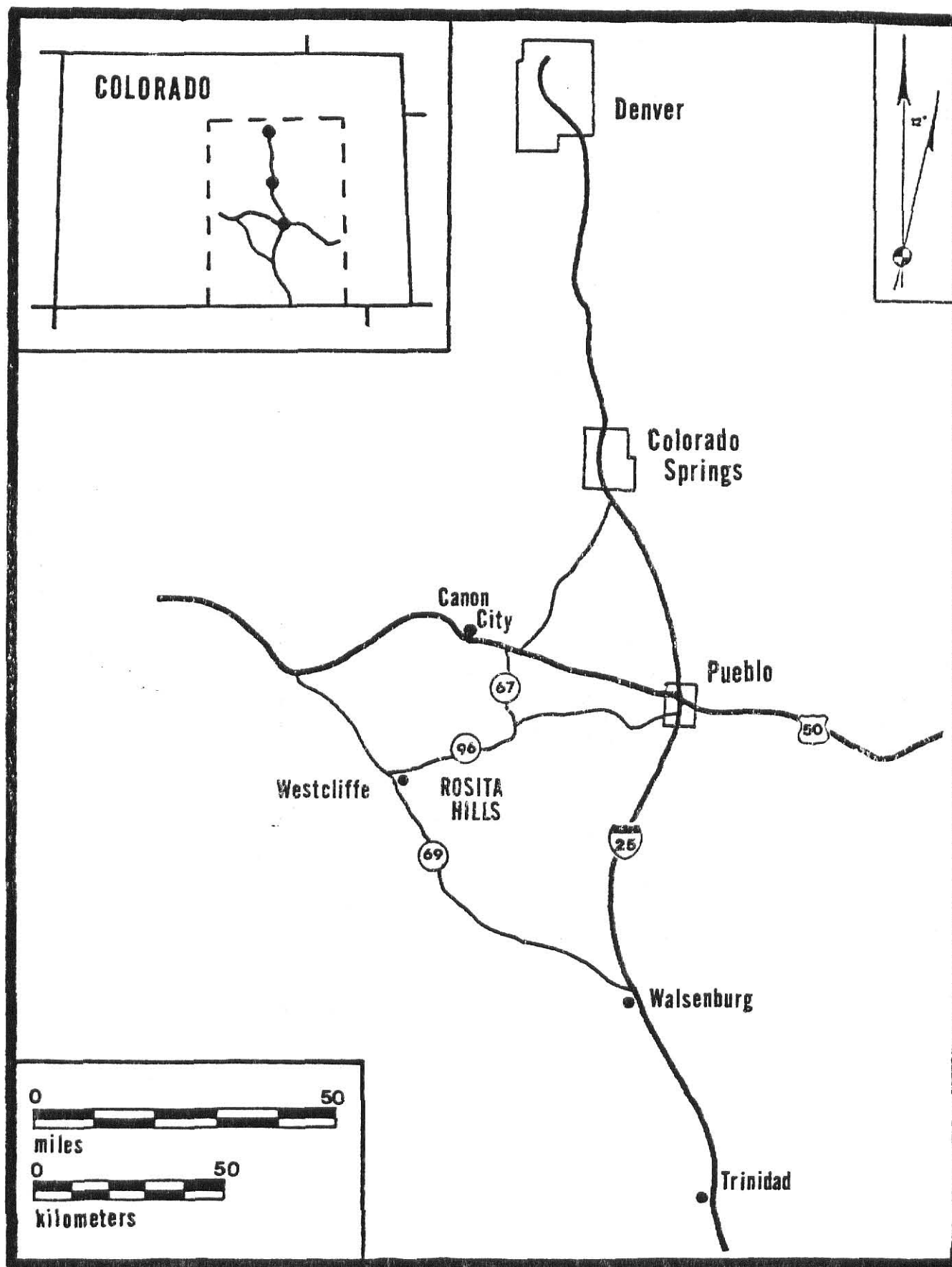


FIGURE 1: Map showing location of the Rosita Hills district.

Petrology of the Rosita Hills

Volcanic District

Field investigations by Siems (1967) and Sharp (1978) have delineated 10 major volcanic lithologic units within the Rosita Hills district, each of which represents a separate eruptive phase. By examining the field relationships among the rock units, they reconstructed the chronological sequence of eruption of the various magma types. In the following discussion the volcanic units of the Rosita Hills are described and arranged in order of decreasing age (Figure 2).

Pre-Volcanic Rocks (YXgg)

The volcanic rocks of the province lie on an erosional surface of Precambrian metamorphic and igneous rocks. These consist of a complex series of interlayered paragneisses, migmatite, and gneiss which is intruded by dikes of albite syenite (Christman et al., 1959). Rocks of this type are exposed primarily on the eastern and northern edges of the province but are also exposed over small areas within the central portion of the district (Siems, 1967).

Rhyolitic Pyroclastic Rocks (Tdh, Trt)

The oldest volcanic rock unit of the suite consists of rhyolitic pyroclastic deposits which are present in the southeastern portion of the province (Siems, 1967). These include air-fall tuffs, tuff breccias, tuff agglomerates, and water-laid tuffs. Directly on these deposits rests a discontinuous but extensive unit of rhyolitic ash-flow tuff

(Trt). The preserved volume of this unit is about a tenth of a cubic mile and the original volume was probably much greater (Siems, 1967). The ash flow tuff contains zones of partial welding, but it is primarily non-welded (Siems, 1967).

Rosita Formation (Tra)

The Rosita Formation represents the altered remains of an andesitic volcanic cone which was the dominant structure of the complex during the early history of the province (Sharp, 1978). This andesitic phase of volcanism probably lasted for several million years prior to the occurrence of large-scale cauldron subsidence (Siems, 1967). The formation is complex and widespread over the northeastern portion of the province and consists primarily of volcanoclastic sediments (conglomerate, sandstone, and mudflow deposits), tephra accumulations, and small lava flows. Most of the unit is significantly altered by hydrothermal activity. The Bassick breccia pipe is located within the Rosita Formation, and it represents an explosive vent. The vent served as a host rock for the deposition of numerous ores including silver and gold tellurides, galena, sphalerite, and tetrahedrite (Siems, 1967).

Hornblende Trachyandesite (Ta)

This unit consists of vents and small flows located in the southwestern portion of the district. The vents and flows are the result of localized volcanism associated with a ring fracture system developed during the subsidence

episode (Sharp, 1978). The rock is porphyritic and contains phenocrysts of plagioclase, hornblende, clinopyroxene, and biotite in a cryptocrystalline groundmass.

Rhyodacite (Tbm)

Rhyodacite occurs in the southeastern portion of the district in the form of domes and associated lava flows. The rock is fine-grained and holocrystalline; it tends to be somewhat altered by weathering and consists of microporphyritic phenocrysts of plagioclase, sanidine, biotite, and hornblende in a microcrystalline groundmass containing interstitial quartz. The unit intrudes and overlies the Rosita Formation (Tra; Siems, 1967).

Rhyolite (Trr)

Extensive rhyolite covers much of the southwestern portion of the district. This unit formed primarily as the result of ring fracture volcanism. It consists of fissure flows, ash flow tuffs, dome structures, and dikes (Sharp, 1978). Eruptions of this material closely followed those of the rhyodacite (Tbm), and it is possible that some of the earlier rhyodacite conduits were reopened to allow the rise of rhyolitic magma to the surface (Siems, 1967). The felsic flows are slightly porphyritic with small phenocrysts of sanidine in a fine-grained groundmass of sanidine and quartz. In many places the glassy flows are altered to zeolite and are green because of the presence of celadonite (Sharp, 1978).

Bunker Hill Trachyandesite (Tb)

Porphyritic trachyandesite is exposed over much of the northwestern portion of the province. It was apparently intruded as stocks and dikes under a shallow cover of older volcanic beds within the cauldron structure, and it may have broken through the surface in some areas (Siems, 1967). The rock is characteristically light grey, and it tends to be very resistant to weathering. Different proportions of plagioclase, sanidine, biotite, hornblende, and clinopyroxene occur in the felsic groundmass.

Syenodiorite (Tbs)

Small intrusive bodies of syenodiorite occur within the Bunker Hill trachyandesite (Tb). Chilled margins occur along some of the syenodiorite wall contacts (Siems, 1967). The unit is generally coarser grained than the other rock units of the suite. The texture varies from porphyritic with cryptocrystalline groundmass to hypidiomorphic-granular. Mineralogically, the syenodiorite consists of plagioclase and clinopyroxene with lesser amounts of sanidine and black oxides.

Latite (Tp)

A fairly large stock of latite magma was emplaced in the southern portion of the cauldron structure following the emplacement of the trachyandesite (Tb) stock. At about the same time, the western half of the district was intruded by numerous latite dikes. The latite dikes cut both the

rhyolite (Trr) and trachyandesite (Tb). The latite is characteristically resistant to weathering and in places is fairly coarse-grained and grades into quartz monzonite. It contains abundant phenocrysts of plagioclase, potassium feldspar, biotite, hornblende, and occasional clinopyroxene in a groundmass of felsic material containing minor interstitial quartz.

Trachyte (Tt)

Two extensive trachyte lava flows and a complex system of radiating trachyte dikes occur within the district. Siems (1967) interpreted these as representing the last major eruptive phase of volcanism within the province. The flows are present in the northeastern quarter of the district within the cauldron structure and overlying the Rosita Formation. The associated dikes intrude the latite (Tp), trachyandesite (Tb), and rhyolite (Trr) (Siems, 1967). The rock consists of large but sparse phenocrysts of sanidine (up to 1 cm in length) and smaller crystals of plagioclase and biotite in a fine-grained groundmass of felsic material that has minor interstitial quartz.

Lamprophyre (Tl)

Lamprophyre dikes of relatively minor volumetric importance occur in the northeast and southwest portions of the district. They are spatially related to the rhyolite (Trr) domes and were emplaced along fractures which probably resulted from the intrusion of the domes (Siems, 1968). The relative age of the lamprophyre intrusions with respect to











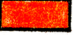











units younger than the rhyolite is not clear. Mineralogically, the lamprophyres are olivine vogesites according to the classification of Rock (1977). They contain small phenocrysts of olivine in a glassy matrix containing minute crystals of plagioclase, clinopyroxene, and amphibole.

Geochronology

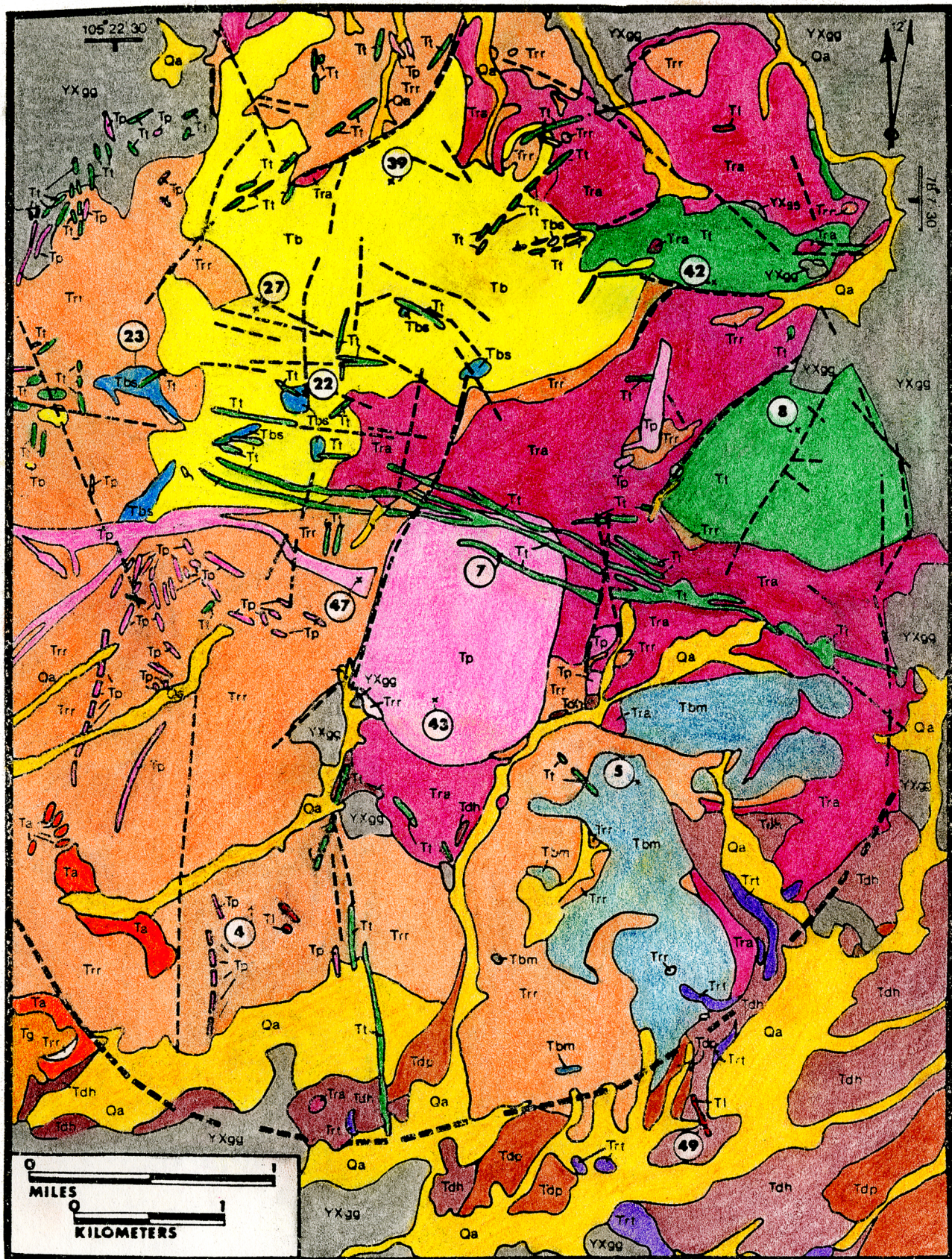
Radiometric age determinations of volcanic rock samples from the Rosita Hills district were conducted by Scott and Taylor (1975) using the $^{40}\text{K}/^{40}\text{Ar}$ method. These ages are listed in Table 1 below:

Table 1: Radiometric age determinations of volcanic rock samples from the Rosita Hills district (Scott and Taylor, 1975)

Trachyte (Tt)	26.4 million years
Rhyodacite (Tbm)	26.7 million years
Rosita Formation (Tra)	29.8 million years
Rhyolite Tuff (Trt)	32.1 million years

		Qa	Unconsolidated Alluvial Deposits (Holocene-Pleistocene)	
		Tg	Gravels on Cut Surfaces (Pliocene)	
 MIOCENE		Tt	Trachyte of Game Ridge	
		Tp	Pringle Latite	
		Tbs	Bunker Trachyandesite - Syenodiorite Phase	
		Tb	Bunker Trachyandesite - Main Body	
		Tl	Lamprophyre	
		Trr	Rhyolite of Rosita Volcano	
		Tbm	Rhyodacite of Bald Mountain	
		Ta	Hornblende Andesite	
 OLIGOCENE		Tra	Rosita Andesite	
		Tdp	Deer Peak Volcanics	 contact
		Tdh	Devil's Hole Formation	 fault
		Trt	Rhyolite Tuff	 probable ringfault
		Trb	Rhyolite of Antelope Butte	 sampling location
		YXgg	Precambrian Metamorphic and Igneous Rocks	

*traced from U.S.G.S. Miscellaneous Investigation Series
Map No. 1-1081 (Sharp, 1978)



EXPERIMENTAL METHODS

Sample Collection and Preparation

Samples of the major rock types exposed within the Rosita Hills district were collected during the summer of 1978. Relatively unaltered specimens which were representative of the range of composition within the suite were chosen for chemical analysis.

The samples included rocks from the following lithological units:

Rhyodacite (Tbm)..... sample RH-5
Rhyolite (Trr)..... sample RH-4
Trachyandesite (Tb)..... samples RH-27 and RH-39
Syenodiorite (Tbs)..... samples RH-22 and RH-23
Latite (Tp)..... samples RH-43 and RH-47
Trachyte (Tt)..... samples RH-7, RH-8, and RH-42
Lamprophyre (Tl)..... sample RH-49

Sampling locations are shown in Figure 2. Thin sections were made of each specimen, and petrographic descriptions of those thin sections are given in Appendix I.

The rock samples were broken with a sledge hammer to obtain fragments with unweathered surfaces. These fragments were placed in a tungsten carbide lined ball mill and crushed to a powder (finer than 200 mesh). Aliquots of this powder were used for chemical analyses.

Atomic Absorption and Flame-Emission Spectrophotometry

The concentrations of the major elements in 12 rock samples were determined by atomic absorption and flame emission spectrophotometry using a Perkin-Elmer model 305B spectrophotometer. The rock samples were dissolved using the lithium metaborate fusion technique described below (Suhr and Ingamells, 1966).

Sample Dissolution Procedure

0.1000 gram powdered sample (± 0.0002 g) was mixed with 0.5000 gram (± 0.0002 g) anhydrous lithium metaborate (LiBO_2) on a weighing paper and the mixture was completely transferred to a small graphic crucible. The crucible was then placed in a muffle furnace at 1000°C for about 15 minutes during which time fusion of the contents occurred. The crucible was then removed from the furnace while the material was still molten, and the contents were poured into a teflon beaker containing precisely 40.0 ml of distilled HCl (2 N). The beaker was then placed on a magnetic stirring plate to facilitate dissolution of the quenched material, and complete dissolution usually occurred within 10 minutes. The solution was filtered to remove particles of graphic greater than $0.45\ \mu\text{m}$ which had been incorporated into the fusion mixture.

Sample Dilutions

It was necessary to dilute the primary solution of each sample four times to attain the various concentrations required for optimum sensitivity of the spectrophotometer.

Table 2 describes the preparation, concentration, and analytical use of each of these solutions. In order to suppress the tendency of the alkali elements to ionize in the flame, these dilutions were made using a stock solution of 1% La as $\text{LaCl}_3 \cdot 6\text{H}_2\text{O}$ (ASC reagent). Water used in preparing this solution was distilled and then passed through a resin column to reduce its ionic concentration to a conductivity of less than $1 \mu\text{mho}$. To monitor the overall effect of contamination from the water and the various reagents used, a "blank" solution was prepared in an identical manner as each of the samples except that no powdered sample was mixed with the LiBO_2 in the initial step.

Standard Solutions

The analyses of the sample solutions consisted of comparing the absorption and emission intensities as measured by the spectrophotometer with those of synthetic standard solutions. These standards were prepared using certified atomic absorption reference solutions obtained from Fisher Scientific Company. The standard solutions contained a similar matrix to that of the sample solutions (LaCl_3 , LiBO_2 , HCl) and were diluted to a range of concentrations within the sensitivity limits of the spectrophotometer for each element. Table 3 describes the preparation, concentration, and use of these standard solutions.

Analytical Precision

Accuracy of the major element determinations was

TABLE 2: Sample solutions used in atomic absorption
and flame-emission analyses

Solution A:

Preparation: initial solution prepared by dissolving the
fused mixture of 0.1 g sample and 0.5 g LiBO_2
in 40 ml HCl (2N)

Concentration: 0.0025 g sample per ml

Use: determination of Ti content

Solution B:

Preparation: dilution of 10 ml of solution A to 50 ml volume

Concentration: 0.0005 g sample per ml

Use: determination of Si, Al, Mg, and Ca contents

Solution C:

Preparation: dilution of 5 ml of solution B to 50 ml volume

Concentration: 0.00005 g sample per ml

Solution D:

Preparation: dilution of 10 ml of solution C to 20 ml volume

Concentration: 0.000025 g sample per ml

Use: determination of K and Na contents

Solution E:

Preparation: dilution of 10 ml of solution C to 30 ml volume

Concentration: 0.0000166 g sample per ml

Use: determination of K and Na contents

note: all dilutions made using La stock solution

TABLE 3: Standard solutions used in atomic absorption and
flame-emission analyses

Solution 1 (stock):

Preparation: dilution of appropriate volumes of Fisher Scientific Co. atomic absorption reference solutions in solution of 1% La as LaCl_3 and 0.5 N HCL

Concentrations: 10 ppm each: Fe, Mg, Ca, Na, K; 40 ppm Al; 1 ppm Mn

Solution 2:

Preparation: dilution of 100 ml of solution 1 plus 40 ml of Si standard reference solution to 200 ml with La solution

Concentrations: 200 ppm Si; 20 ppm Al; 1 ppm Mn; 5 ppm each: Fe, Mg, Ca, Na, K

Solution 3:

Preparation: dilution of 50 ml of solution 2 to 100 ml with La solution

Concentrations: 100 ppm Si; 10 ppm Al; 0.5 ppm Mn; 2.5 ppm each: Fe, Mg, Ca, Na, K

Solution 4:

Preparation: dilution of 10 ml of solution 1 to 100 ml with La solution

Concentrations: 1 ppm each: Fe, Mg, Ca, Na, K; 4 ppm Al; 0.2 ppm Mn

Solution 5:

Preparation: dilution of 10 ml of solution 1 to 200 ml with La solution

Concentrations: 0.5 ppm each: Fe, Mg, Ca, Na, K; 2 ppm Al; 0.1 ppm Mn

(intermediate and more dilute standards were made in manner similar to solutions 4 and 5)

monitored using U.S.G.S. standard rocks. These were dissolved in the same manner as the samples and analyzed using the same method. The values obtained are compared with those of Flanagan (1976) in Table 4 below.

TABLE 4: Comparison of analyses of U.S.G.S. standard rocks in this study with values reported by Flanagan (1976)

	Flanagan	This Study	Flanagan	This Study	Flanagan	This Study
	G-2	G-2	BCR-1	BCR-1	AGV-1	AGV-1
SiO ₂	69.19	68.17	54.48	53.22	58.99	59.04
Al ₂ O ₃	15.34	15.45	13.65	13.49	17.01	16.79
Fe ₂ O ₃ *	2.76	2.72	13.50	13.57	6.80	6.72
K ₂ O	4.51	4.54	1.68	1.73	2.89	2.94
Na ₂ O	4.15	4.14	3.31	3.34	4.33	4.35
CaO	1.98	1.93	6.95	7.00	4.98	4.86
MgO	0.78	0.76	3.28	3.36	1.49	1.43
TiO ₂	0.53	0.62	2.23	2.10	1.08	1.15

*representing total Fe content

Instrumental Neutron-Activation Analysis

Concentrations of the rare earth elements and other trace-elements listed in Table 12 were determined by instrumental neutron activation analysis. The procedure was based on that of Gordon et al. (1968) and Jacobs et al. (1977) with slight modifications as discussed in Kilbane (1978). A brief outline of the method is summarized below.

Instrumentation

Samples were irradiated for four hours in a General Atomic Triga Mark II experimental reactor with a flux of approximately 10^{13} neutrons/cm²/second. The samples were subsequently radioassayed for gamma radiation using a Ge(Li) detector and Canberra model 8180 multichannel analyzer. The analyzer is equipped with a 4096-channel memory unit which recorded the gamma ray spectrum of each radioactive sample in such a way that there was a linear correlation between increasing channel number in the memory and increasing energy of the gamma ray emissions. This correlation was calibrated using radioactive sources of ¹⁵²Eu (.122 meV and .344 meV) and ⁶⁰Co (1.332 meV). The spectra was transferred to magnetic tapes for computer processing.

Procedure

Groups of five samples were irradiated simultaneously with a primary standard (Canada Certified Reference Materials Project reference soil SO-4). About 0.25 gram (\pm .0002 g) of the powdered material was weighed into small polyethylene

vials. The vials were sealed with a warm soldering gun to make them waterproof in the reactor pool. About 75 mg (\pm 0.1 mg) of analytical grade iron wire was wrapped spirally around the outside of each vial to serve as a monitor of neutron flux variations among samples during irradiation. About four days after irradiation, samples were transferred from the vial to small plastic bags (2 cm x 2 cm) and mounted on index cards. Samples were radioassayed three times after irradiation (after 5, 10, and 40 day intervals) to obtain optimum resolution of the gamma-ray energies of interest.

Calculations

Calculations of the concentrations of the trace elements consisted of comparing the emission rates of particular gamma ray energies in each sample to those of the primary standard. This involved measurement of the areas of peaks on the analyzer spectrum corresponding to gamma radiation energies of interest. Peak area determinations were made using a computer program adopted from Jacobs et al. (1977). The program calculates peak areas and translates these into counts per second values and sample/standard ratios taking into account changes in activity due to decay during count sets. Data input includes the gamma-ray spectra of the standard plus five samples recorded on magnetic tape, the actual time elapsed during radioassay, the "live time" of the analyzer during radioassay, and the calibration of the spectrum. Output is in the form of sample/standard activ-

ity ratios for elements of interest. These ratios must be corrected for reactor flux variations and weight differences between sample and standard. This was done using the following equation:

$$C_s = (C_{st}) \left(\frac{\text{st. wt.}}{\text{s. wt.}} \right) \left(\frac{\text{st. Fe}}{\text{s. Fe}} \right) \left(\frac{\text{s.}}{\text{st.}} \right)$$

where:

C_s = concentration of element in sample

C_{st} = concentration of element in standard

$\frac{\text{st. wt.}}{\text{s. wt.}}$ = standard/sample weight ratio

$\frac{\text{st. Fe}}{\text{s. Fe}}$ = ratio of the activity of the iron wire flux monitors (standard/sample)

$\frac{\text{s.}}{\text{st.}}$ = sample/standard activity ratio

Analytical Precision

Accuracy of the concentrations determined by this method was monitored using secondary standards which were analyzed in the same manner as the rock samples. The results of the analysis of U.S.G.S. standard BCR-1 is compared to assays by other analysts in Table 5.

Precision of the measurements varies depending on the element measured. The precision is best for La, Ce, Sm, and Co for which the uncertainty in the measurement is less than 10 percent. Eu, Yb, Th, and Lu concentrations are somewhat less precise with uncertainties of as much as 13 percent. Ba and Tb measurements are the least precise with uncertainties of about 15 percent.

TABLE 5: Trace-element concentrations (ppm) in U.S.G.S. standard BCR-1 as determined by neutron activation in this study compared to analyses of others

	This study	Flanagan (1976)	Gordon et al. (1968)	Koch (1978)
La	27	26	23	28
Ce	54	53	46	50
Sm	6.8	6.6	5.9	6.5
Eu	2.1	1.9	2.0	2.0
Tb	1.1	1.0	1.0	1.0
Yb	3.4	3.2	3.2	3.3
Lu	0.53	0.55	0.60	0.62
Ba	577	675	-	-
Sc	30	33	-	-
Co	37	38	-	-
Hf	5.1	4.7	-	-
Th	7.2	6.0	-	-

Mass Spectrometry

Strontium isotope ratios were determined by mass spectrometry following the procedures of Chaudhuri (1966) and Chaudhuri and Brookins (1969). A Nier type mass spectrometer (Nuclide Corporation Model 6-60-S) with a 60° sector and 6 inch radius was used in the analyses.

Sample Preparation

Based on strontium concentrations in the rock samples as determined by X-ray fluorescence, calculations were made to determine the weight of powdered sample required to yield approximately 15 micrograms of strontium. This amount was placed in a clean 10 ml teflon dish and wetted with a few ml of distilled deionized water. Then approximately 20 ml hydrofluoric acid and 2 ml perchloric acid were added. The dish was placed on a hot plate for several hours to facilitate dissolution of the sample and to evaporate the hydrofluoric acid leaving a perchlorate precipitate. The precipitate was then redissolved in about 20 ml of 2N hydrochloric acid, and the solution was placed on a hot plate to evaporate it to about 15 ml. The solution was allowed to cool for several days to allow rubidium to precipitate as RbClO_4 which was subsequently removed by filtering.

The strontium content of the filtered solutions were concentrated using cation exchange columns filled with a cross linked organic resin (Dowex 50W-X8). The columns were precleaned by passing about 25 ml 2N hydrochloric acid through

them, and the tops of the resin were leveled prior to each separation. The filtered sample solutions were placed in the columns and allowed to penetrate the resin. Then 2N hydrochloric acid was added in 10 ml aliquots. After 50 ml HCl had passed through the columns, the strontium had migrated to the bottom of the column. In order to isolate the strontium, subsequent solution passing through the columns was collected in 5 ml aliquots which were then allowed to evaporate. Visual examination of the resulting precipitates indicated which aliquots contained most of the strontium due to the white color of SrCl_2 . The two beakers which appeared to have the most strontium were selected and a few ml of HCl were added to each to redissolve the precipitate. The solutions were then combined, transferred to small glass beakers and evaporated to dryness. Each sample was then heated over a flame for a few seconds to burn off any organic residue present from the columns. The residues were subsequently redissolved in 2 ml of 3N nitric acid and the solutions were evaporated onto tantalum filaments. The tantalum filaments served as an ion source in the mass spectrometer.

Sample Analysis

Strontium isotope ratios were determined by comparing the abundance peaks of isotope masses 86, 87, and 88. Each of these mass peaks were measured 36 times for each sample (in sets of 6 each) and the sum of the abundance intensities for each set was used for calculating the $^{87}\text{Sr}/^{86}\text{Sr}$ and $^{86}\text{Sr}/^{88}\text{Sr}$ ratios. The $^{86}\text{Sr}/^{88}\text{Sr}$ ratio is constant in nature so this

was used as a monitor of the accuracy of the $^{87}\text{Sr}/^{86}\text{Sr}$ ratio. A small correction factor was used based on the value of the measured $^{86}\text{Sr}/^{88}\text{Sr}$ ratio to standardized the $^{87}\text{Sr}/^{86}\text{Sr}$ with the measurements of other analysts.

X-ray Fluorescence

Concentrations of Rb and Sr were determined by X-ray fluorescence using a Phillips 1410 X-ray spectrometer (molybdenum target, LiF analyzing crystal). Five U.S.G.S. standard rocks (W-1, BCR-1, AGV-1, G-2, and GSP-1) were used to construct a linear regression of counts per second versus element concentration. Instrument settings and Compton scattering peaks utilized are listed in Table 6.

TABLE 6: Instrument settings and Compton scattering peaks utilized in Rb and Sr determinations by X-ray fluorescence

kilovolts	50	baseline	2.1
milliamps	50	window	2.1
<u>Compton scattering peaks:</u>			
Rb:	38.00°	2	0
Sr:	35.85°	2	0

RESULTS

Major Elements

The major-element contents of the rock samples analyzed in this study (Appendix II) are given in terms of weight-percent oxides although actual determinations consisted of measurement of the cation concentrations in the samples. C.I.P.W. normative mineral compositions were calculated for each sample using the major-element data (Appendix II). The data are plotted in variation diagrams in Figures 3 through 7 together with previous analyses from Cross (1896; Appendix II).

Concentrations of SiO_2 within the samples of the suite span a nearly continuous range from 45.7 percent in the lamprophyre (Tl) to 74.5 percent in one of the rhyolite samples (Trr). SiO_2 concentrations correlate in a nearly linear fashion with the differentiation index (D.I. = normative $Q + \text{or} + \text{ab} + \text{ne}$) of Thornton and Tuttle (1960; Figure 3).

K_2O concentrations within the suite fall primarily within the range of 3.5 percent to 7.0 percent (Figure 4). A gradual continuous increase in K_2O corresponding to increasing SiO_2 can be observed in the compositions of trachyandesite (Tb), latite (Tp), and trachyte (Tt). Considerable differences occur between the trachyte (Tt) K_2O concentrations and those of the rhyodacite (Tbm), although the rocks have similar SiO_2 concentrations. K_2O concentrations within the rhyolite (Trr) samples are intermediate between those of the rhyodacite (Tbm) and trachyte (Tt). The lamprophyre (Tl) contains low

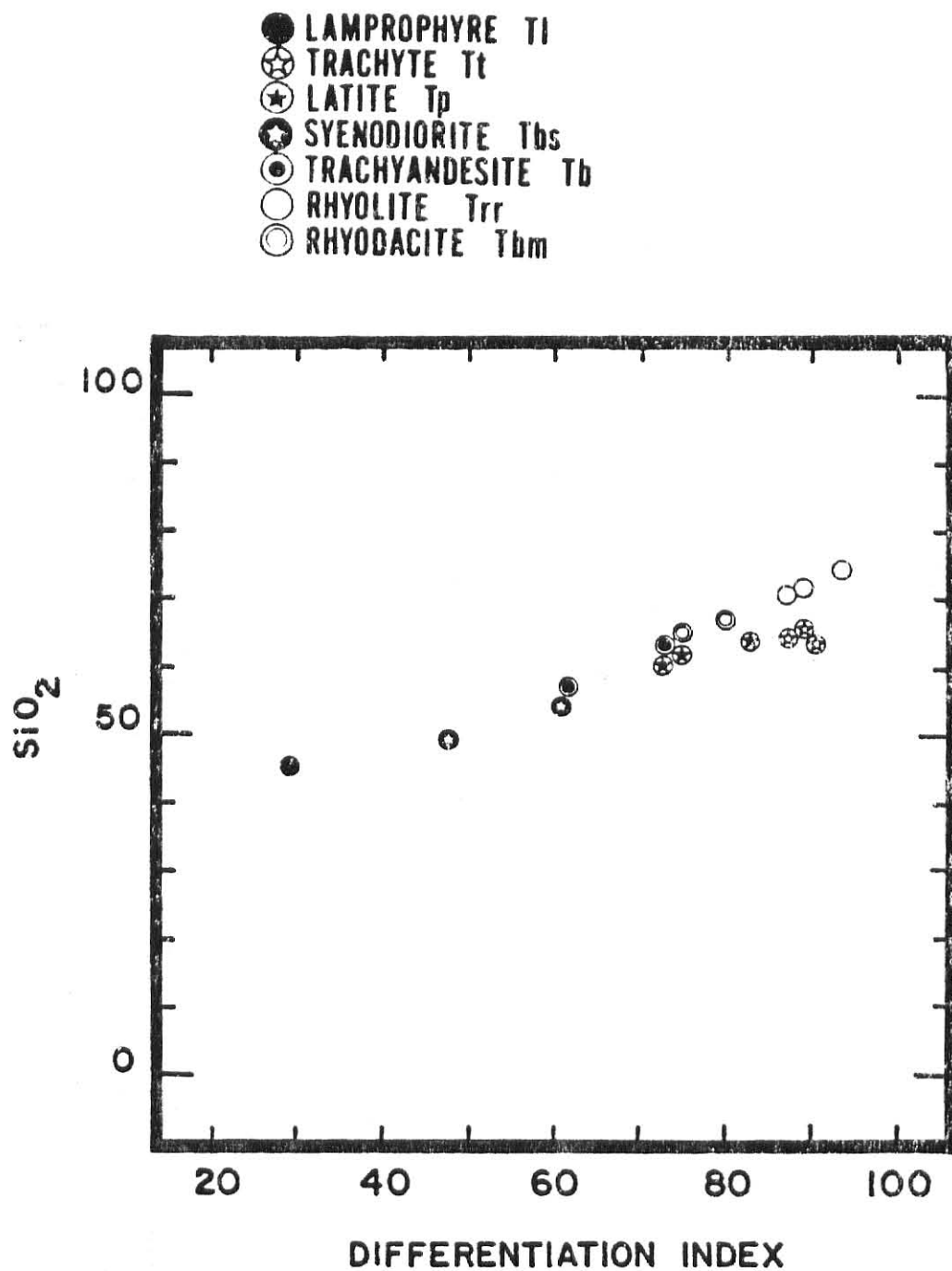


FIGURE 3: Variation in SiO₂ concentrations (weight percent oxide) with respect to the differentiation index (D.I. = normative Q + or + ab + ne) among samples of the Rosita Hills volcanic rock suite.

concentrations of K_2O compared to the rest of the suite.

Somewhat less variation is seen in the concentrations of Na_2O in the samples analyzed. Na_2O concentrations generally fall between 4.0 percent and 6.0 percent with the exception of the lamprophyre (Tl) and rhyolite (Trr) samples which contain slightly less sodium (Figure 5).

Concentrations of CaO , Fe_2O_3 , and MgO within samples of the suite exhibit considerable variation ranging from less than 1.0 percent to greater than 10.0 percent. A nearly linear correlation can be seen between decreasing concentrations of these oxides and the concentration of SiO_2 (Figure 6). A similar decrease is evident in the concentrations of MgO among samples (Figure 6). The exception is that the lamprophyre (Tl) exhibits anomalously high concentration in the MgO plot and does not plot with the trend followed by the rest of the suite.

Smooth trends with little scatter are also present in the AFM (alkali-iron-magnesium) diagram (Figure 6) and the sodium-potassium-calcium oxide diagram (Figure 7). The data graphed within the AFM diagram followed a trend that is very similar to the average trend exhibited by the Cascade calc-alkaline suite (Carmichael, 1964). Progressive enrichment in the alkalis occurs with no relative enrichment in iron. Figure 7 illustrates that the K_2O/Na_2O ratios are similar in the syenodiorite (Tbs), trachyandesite (Tb), and latite (Tp) but increase with progressive alkali enrichment in the trachyte (Tt) and rhyolite (Trr). There is

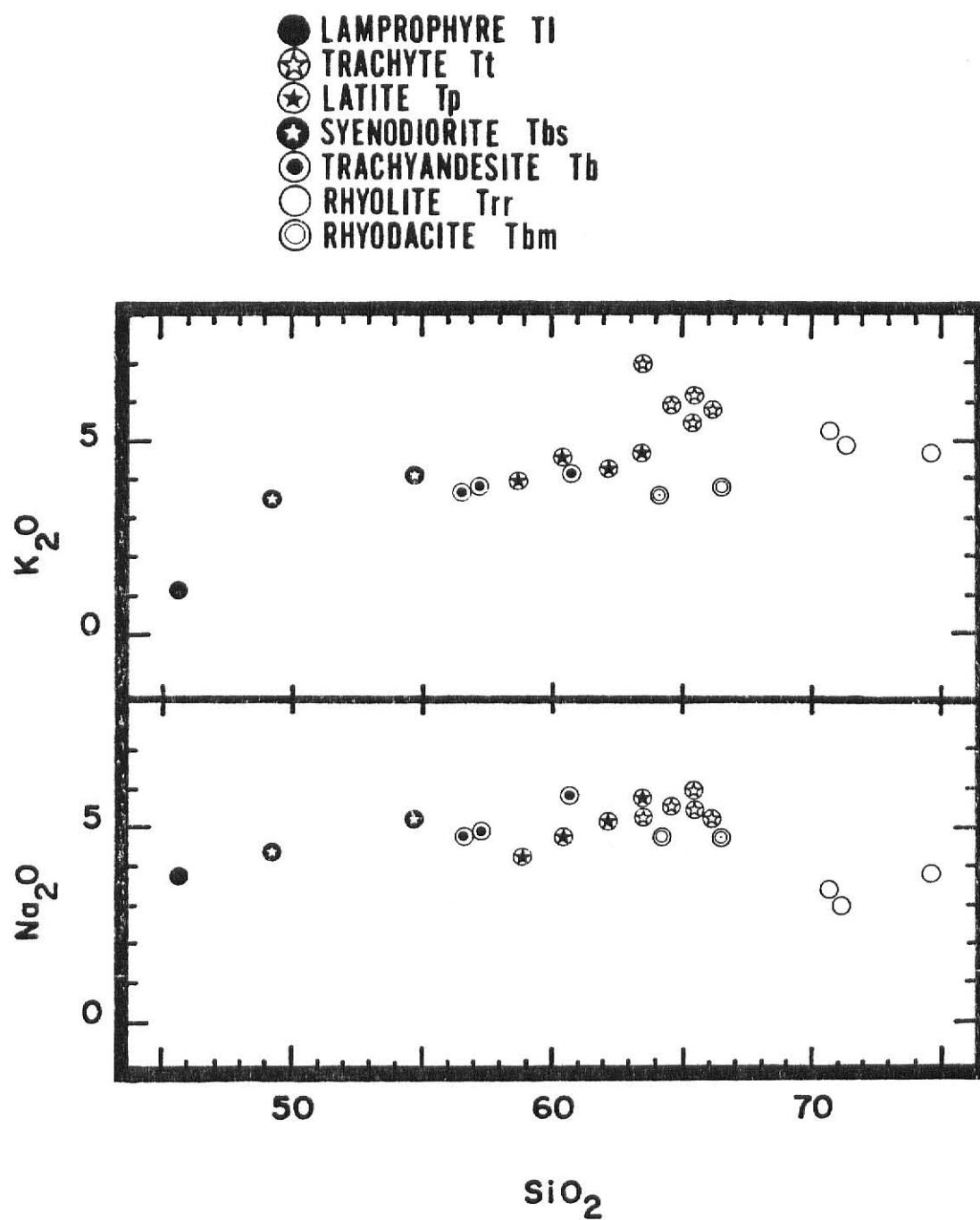


FIGURE 4: Variations in K_2O and Na_2O concentrations among samples of the Rosita Hills volcanic rock suite with respect to SiO_2 contents.

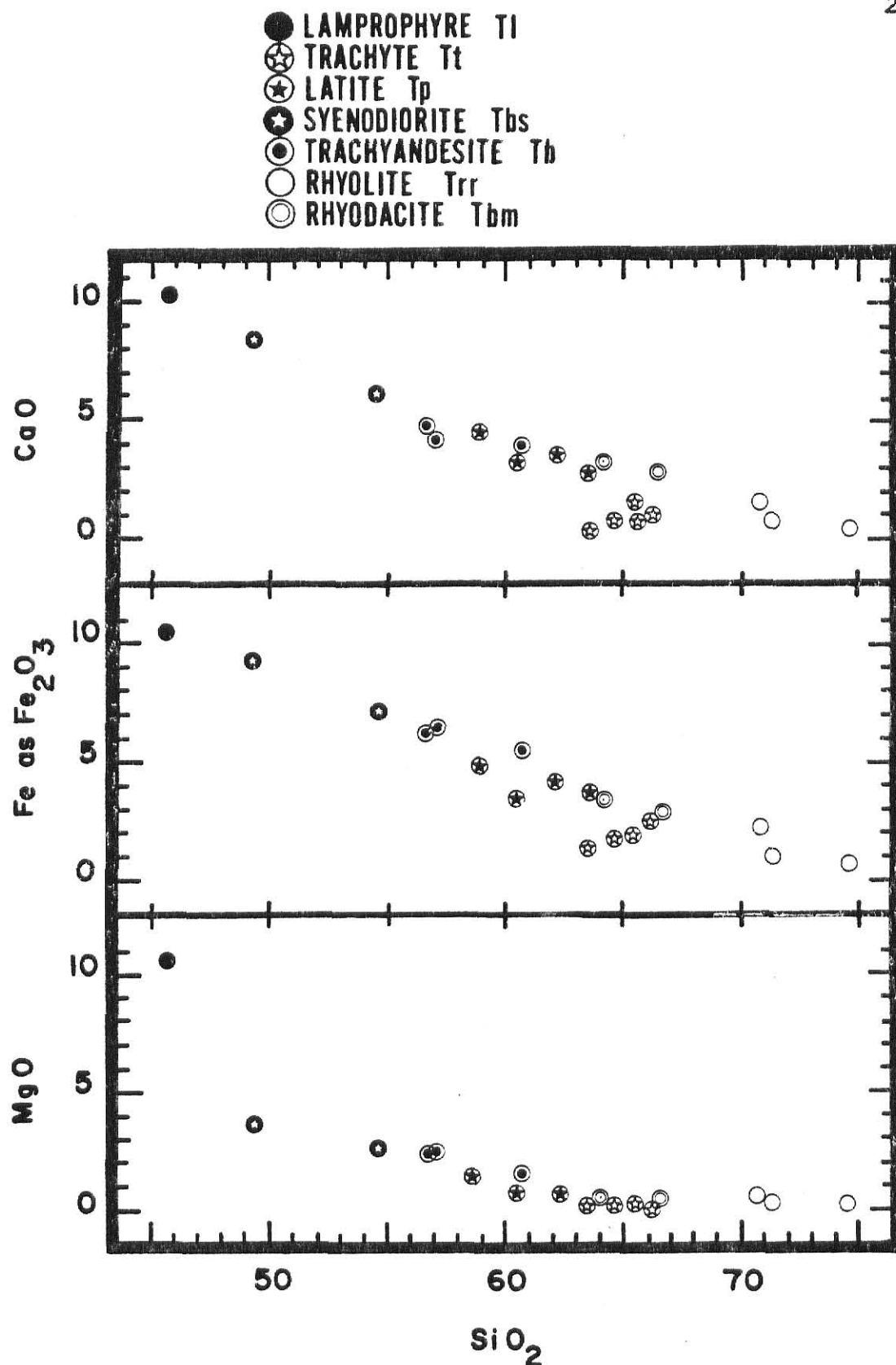


FIGURE 5: Variation in Fe_2O_3 (representing total Fe content), CaO and MgO concentrations among samples of the Rosita Hills volcanic rock suite with respect to SiO_2 contents.

considerable compositional gap evident on both of these graphs between the lamprophyre (Tl) and the rest of the suite.

Normative quartz is present in the latite (Tp), trachyte (Tt), rhyodacite (Tbm), and rhyolite (Trr) as well as in trace amounts in the trachyandesite (Tb). However, quartz is absent in the norms of the syenodiorite (Tbs) and the lamprophyre (Tl). Instead they contain normative nepheline. Normative olivine is present in the lamprophyre (Tl), the syenodiorite (Tbs), and one of the trachyandesite (Tb). The rhyodacite (Tbm), trachyandesite (Tb), syenodiorite (Tbs), and lamprophyre (Tl) all contain normative diopside that is absent in the normative mineralogies of the rest of the units of the suite. Normative anorthite contents are less than An_8 among samples of latite (Tp), trachyte (Tt), and rhyolite (Trr), and range from An_{15} to An_{22} among samples of rhyodacite (Tbm) and trachyandesite (Tb). Normative anorthite contents of the syenodiorite (Tbs) and lamprophyre (Tl) are considerably higher than the rest of the suite with an average of An_{49} for the syenodiorite (Tb) and An_{59} for the lamprophyre (Tl). All of the units analyzed with the exception of lamprophyre (Tl) and syenodiorite (Tbs) contain minor amounts of normative hypersthene. Orthoclase is an important normative component in all of the samples and ranges from 6 percent to greater than 40 percent of the norm.

The tendencies for relatively high concentrations of the alkali elements (particularly K) within samples of the Rosita Hills suite compared to other calc-alkaline provinces is

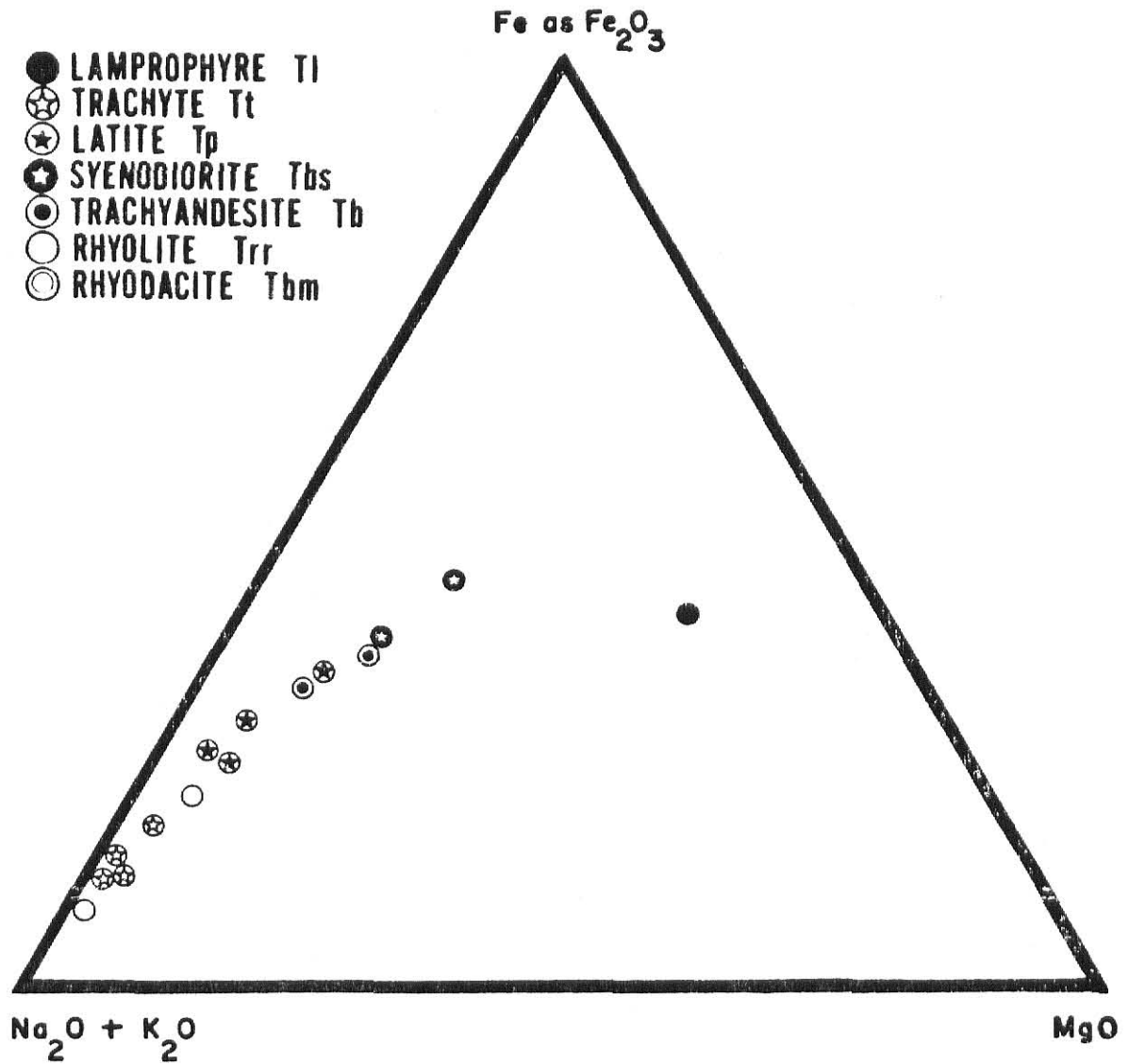


FIGURE 6: Alkali-iron-magnesium triangular variation diagram of samples from the Rosita Hills volcanic rock suite.

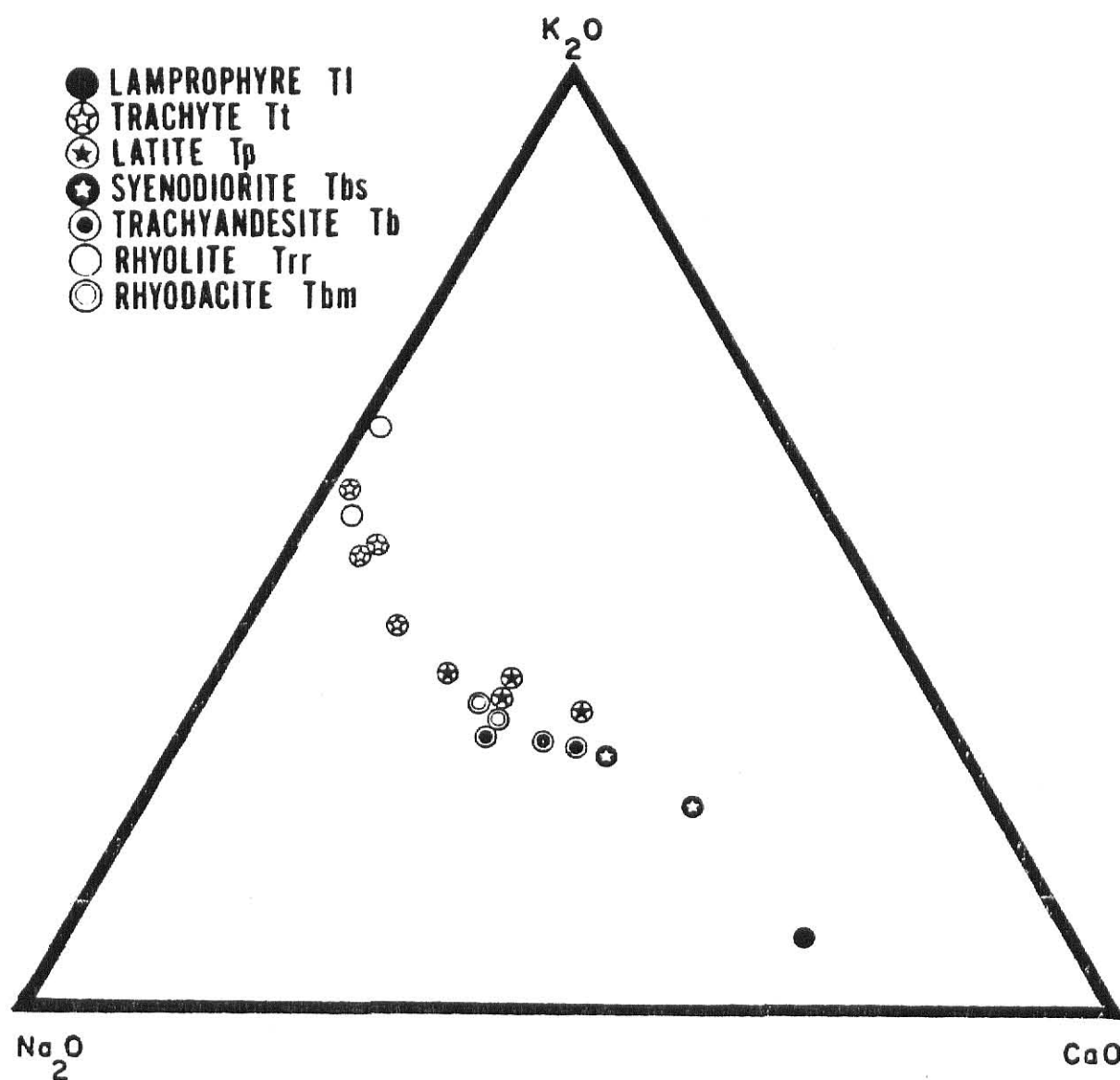


FIGURE 7: Na_2O - K_2O - CaO triangular variation diagram of samples from the Rosita Hills volcanic rock suite.

illustrated by the alkali-lime index of Peacock (1931). In Figure 8, this index is determined by plotting weight percent oxide concentrations of total alkalies ($\text{Na}_2\text{O} + \text{K}_2\text{O}$) versus SiO_2 and CaO versus SiO_2 on the same graph. The index is represented by the SiO_2 concentration at which the two compositional trends intersect and is used as a comparison among rock suites by using the following adjectives:

index greater than 61 calcic
 index between 56 and 61 calc-alkalic
 index between 51 and 56 alkali-calcic
 index less than 51 alkalic

The data in Figure 8 indicate an alkali-lime index of somewhere between 51 and 53 which would correspond to a classification of "alkali-calcic."

On several of the major element variation diagrams, there is an indication of some divergence in the trends. This is especially evident in the plots of SiO_2 versus differentiation index (Figure 3), K_2O versus SiO_2 (Figure 4), and CaO versus SiO_2 (Figure 5). On these diagrams, the rhyodacite (Tbm) and rhyolite (Trr) form a trend which diverges from the variation trend of trachyandesite (Tb), latite (Tp), and trachyte (Tt) compositions. The lamprophyre (Tl) composition plots anomalously to the rest of the suite on the AFM diagram (Figure 6), and K_2O versus SiO_2 plot (Figure 4) and the MgO variation diagram (Figure 5).

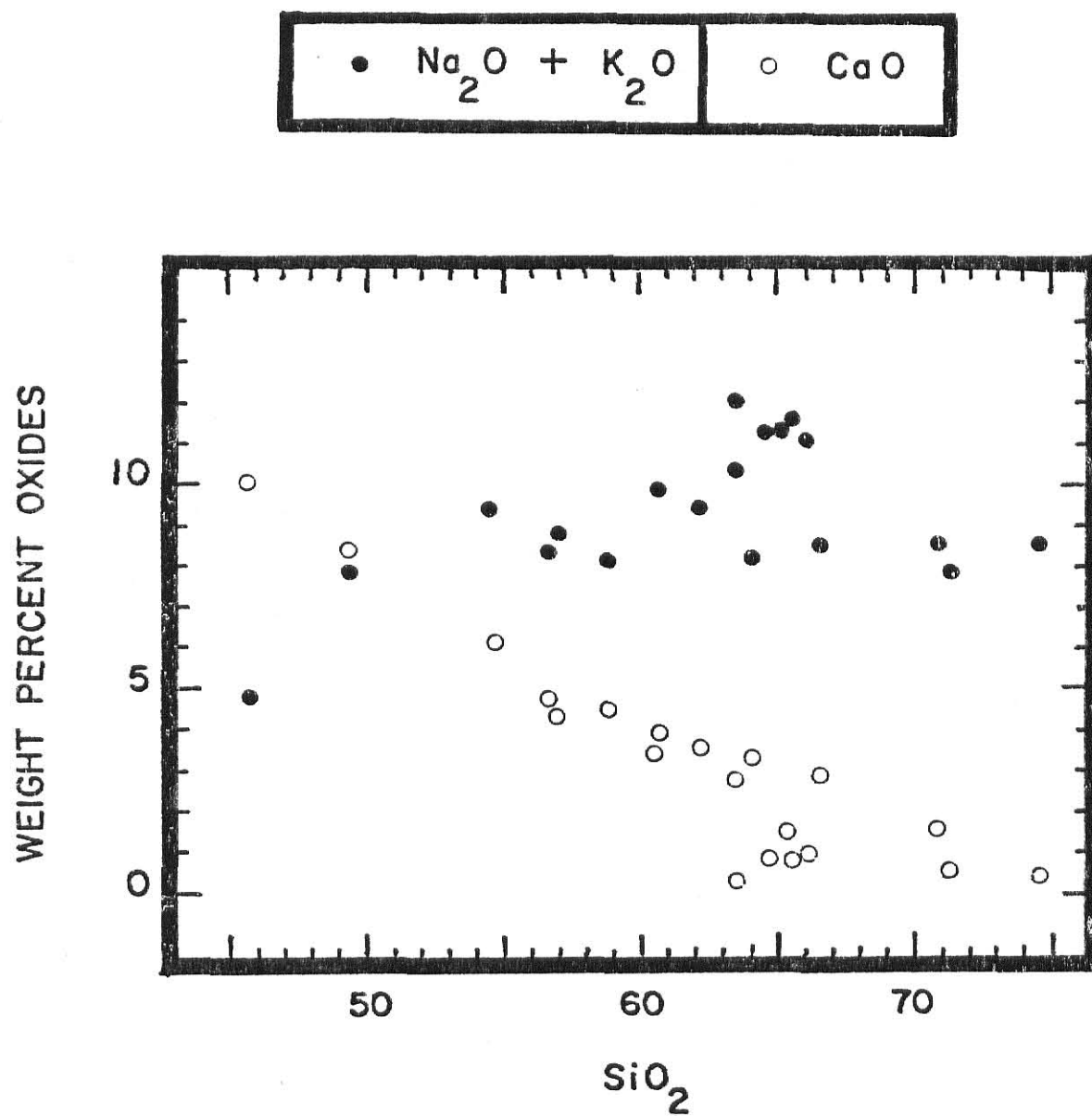


FIGURE 8: Alkali-lime index plot of the Rosita Hills volcanic rock suite.

Trace Elements

Concentrations of Sr and Rb in rock samples from the Rosita Hills district are listed in Table 15 in Appendix II. The values are plotted versus SiO_2 concentrations in the samples in Figure 9. There is a general trend towards decreasing Sr corresponding to increasing SiO_2 contents among the samples. The rhyodacite (Tbm) sample is anomalous to this trend. Rb generally increases among samples corresponding to increasing SiO_2 concentrations. The rhyodacite sample plots away from the main trend on this variation diagram also.

K/Rb ratios are plotted versus K_2O in the manner of Shaw (1970) in Figure 10. There is a gradual decreasing trend in the K/Rb value corresponding to increasing K_2O in samples of trachyandesite (Tb), latite (Tp), and trachyte (Tt). K/Rb values of rhyodacite (Tbm), rhyolite (Trr), and lamprophyre (Tl) do not fit this trend.

Concentrations of Sc, Ba, Th, Co, and Hf in Rosita Hills samples are listed in Table 14. Concentrations of Sc, Ba, and Th are plotted versus SiO_2 in Figure 11. Sc tends to decrease with increasing SiO_2 among samples. The lamprophyre (Tl) sample has a considerably higher Sc concentration than the rest of the suite. Th tends to increase with increasing SiO_2 with the exception of the rhyodacite (Tbm) sample. Ba concentrations increase corresponding to increasing SiO_2 among the more mafic members of the suite. In the more silicic rock types, however, Ba decreases with increasing SiO_2 .

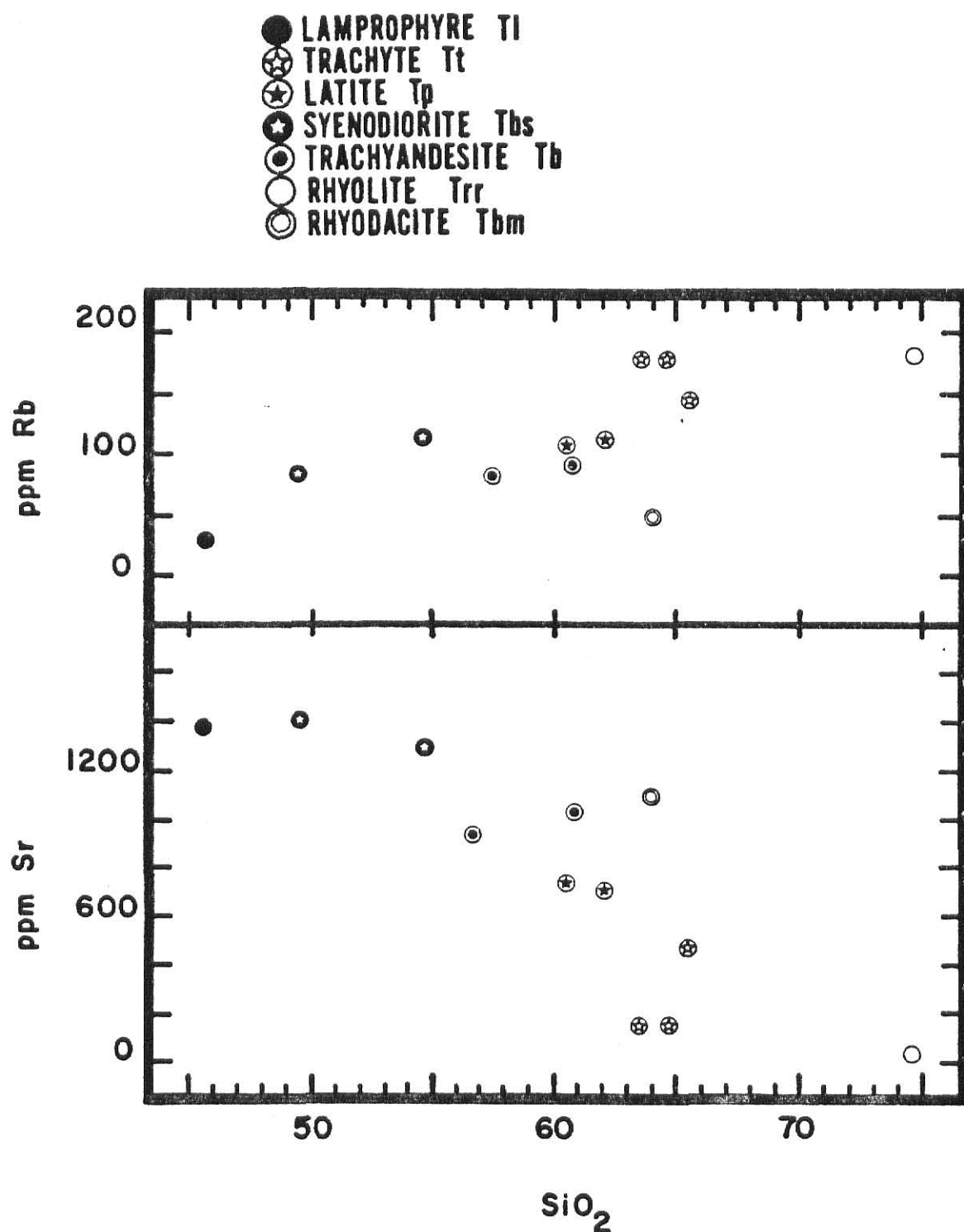


FIGURE 9: Variation in Sr and Rb concentrations (ppm) among samples of the Rosita Hills volcanic suite with respect to SiO₂ contents (weight-percent oxides).

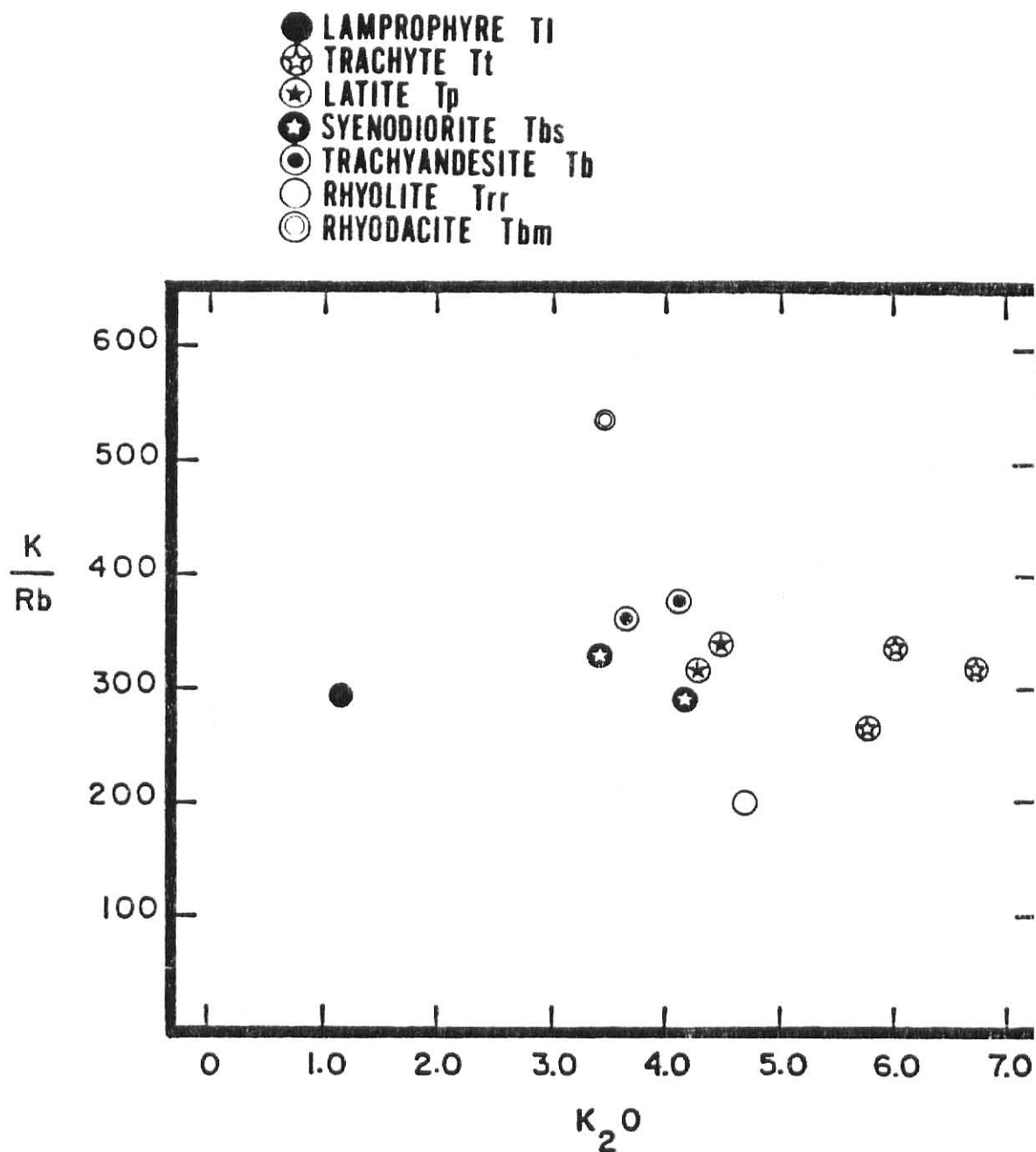


FIGURE 10: Variations in the K/Rb ratio among samples of the Rosita Hills volcanic rock suite with respect to K_2O concentrations (weight-percent oxides).

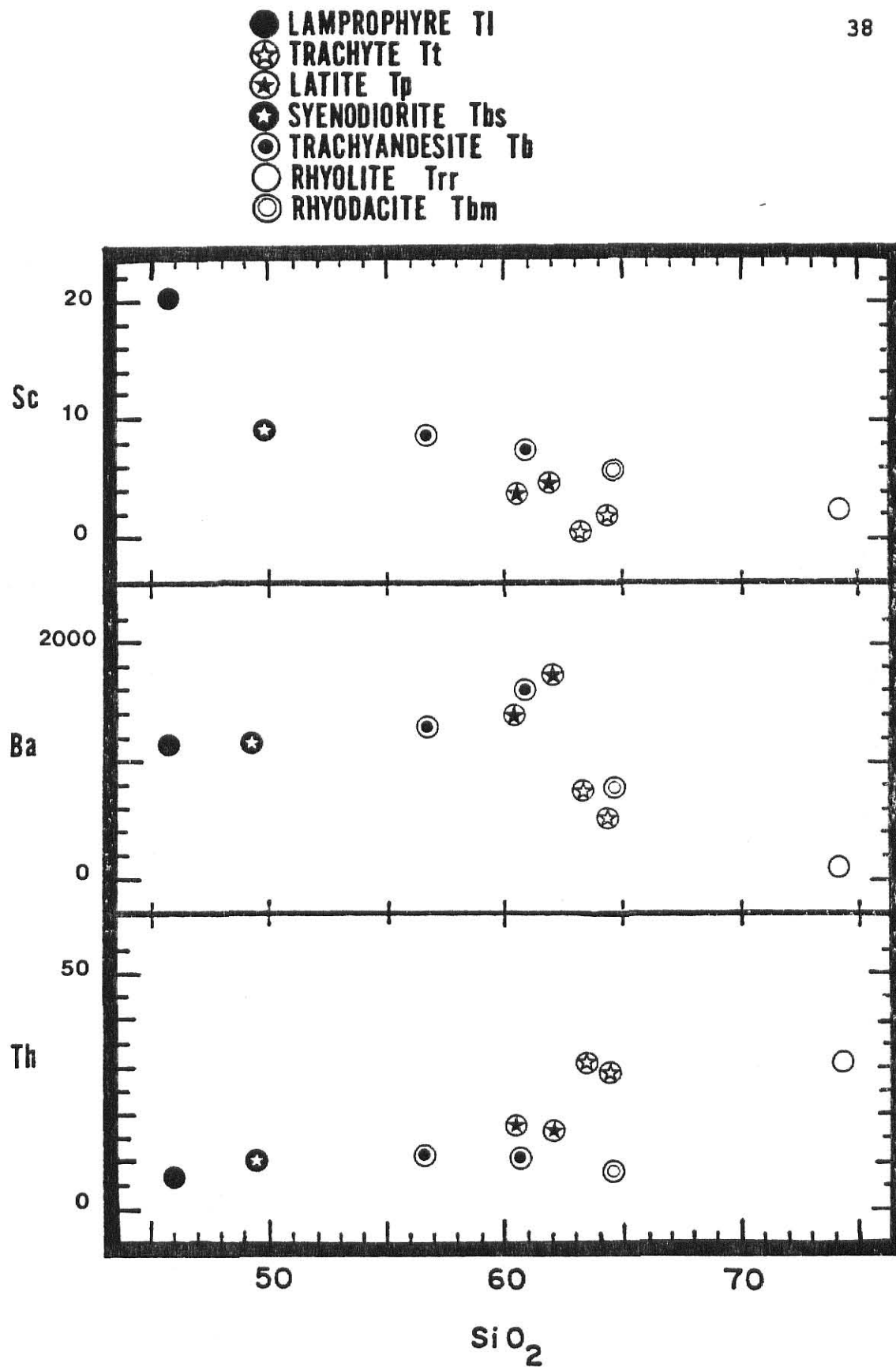


FIGURE 11: Variation in Sc, Ba, and Th concentrations (ppm) among samples with respect to SiO₂ contents.

Rare Earth Elements

REE (rare earth element) concentrations in 10 samples from the Rosita Hills are given in Table 14 in Appendix II. REE distributions are plotted normalized to chondritic meteorites in the manner of Haskin et al. (1968) in Figures 12a through 12d.

All of the samples analyzed have fairly high REE concentrations. The trachyandesite (Tb) and syenodiorite (Tbs) samples have the highest REE contents of the suite with Σ REE values ranging from 260 ppm to 360 ppm. The total REE contents of the latite (Tp), trachyte (Tt), and lamprophyre (Tl) samples are similar to one another and range from 270 ppm to 285 ppm. The rhyodacite (Tbm) and rhyolite (Trr) samples have the lowest total REE concentrations with Σ REE values of 147 ppm and 126 ppm respectively.

All samples have normalized REE distributions which are enriched in the light REE (La, Ce) with respect to the heavy REE (Yb, Lu). Chondrite normalized La/Lu ratios range from 18 to 24 for most samples. The rhyolite (Trr) sample is significantly less fractionated (La/Lu = 8) than the rest of the samples. The lamprophyre (Tl) is the most fractionated of the samples analyzed (La/Lu = 30).

Negative Eu anomalies occur in the normalized REE distributions of the rhyolite (Trr) and trachyte (Tt) samples. An indication of a slight negative Eu anomaly is detectable in the REE distributions of the latite (Tp) samples.

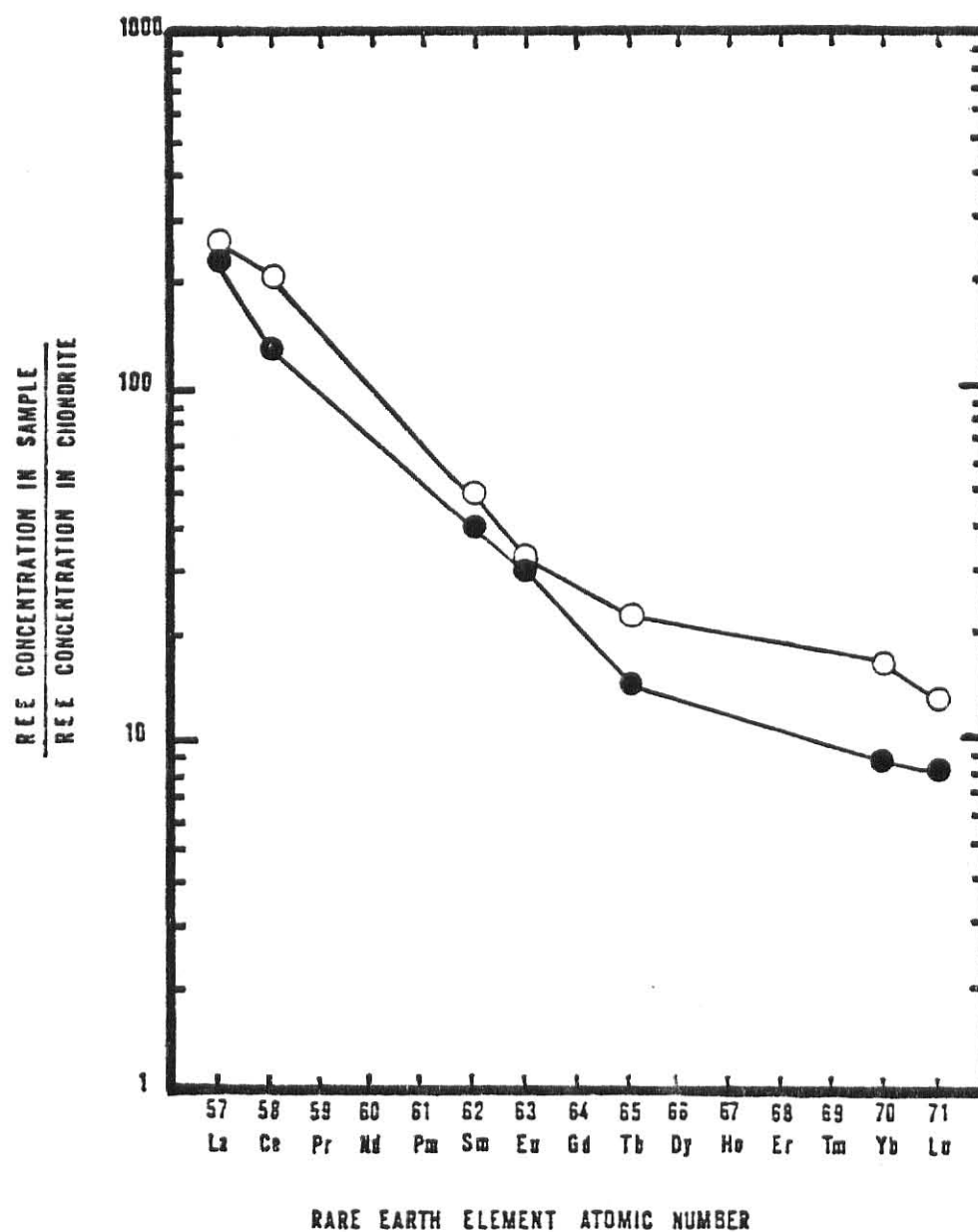


FIGURE 12a: Chondrite-normalized REE distribution of:

SYENODIORITE (○) sample RH-22

LAMPROPHYRE (●) sample RH-49

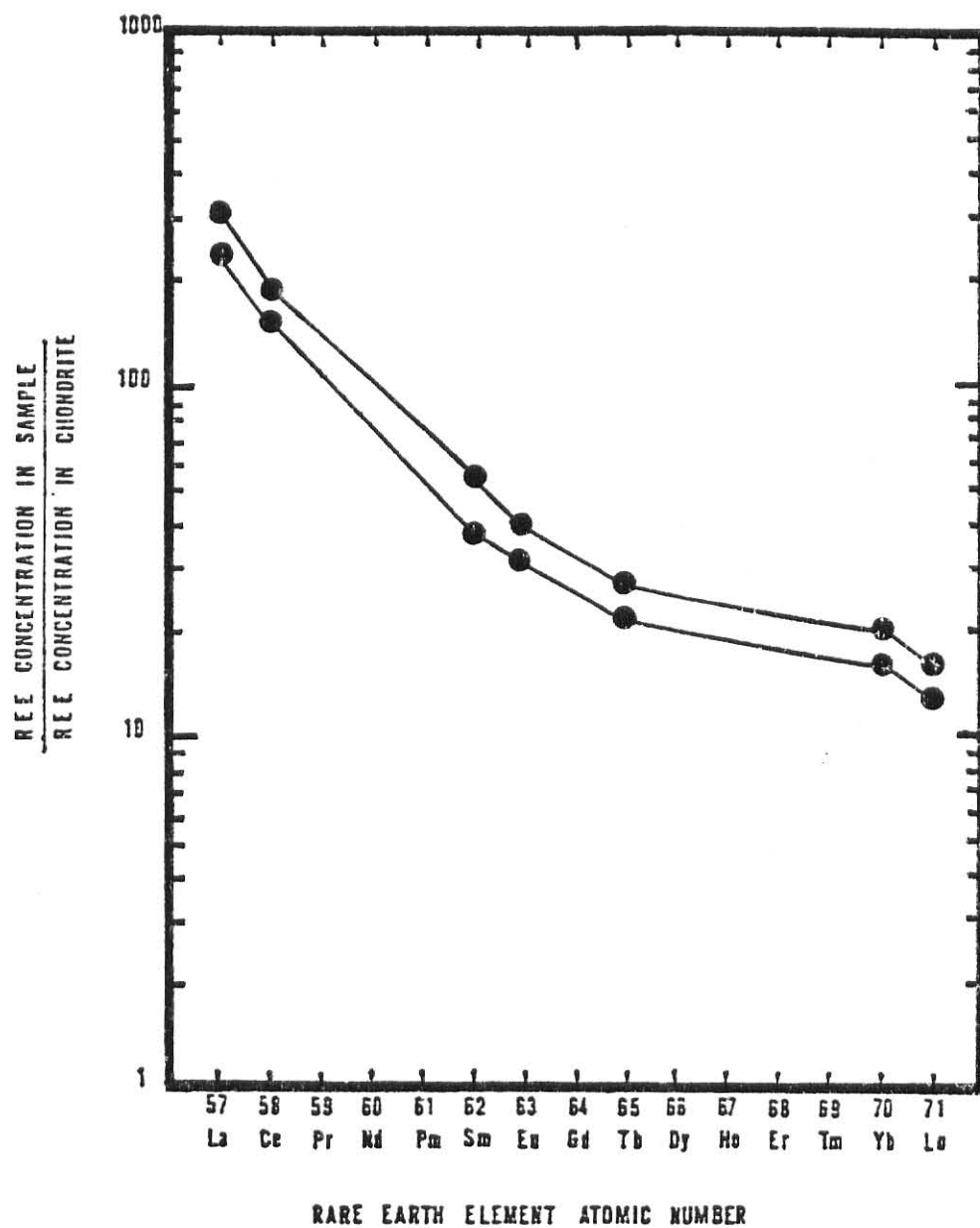


FIGURE 12b: Chondrite-normalized REE distributions of:
TRACHYANDESITE samples RH-39 and RH-27

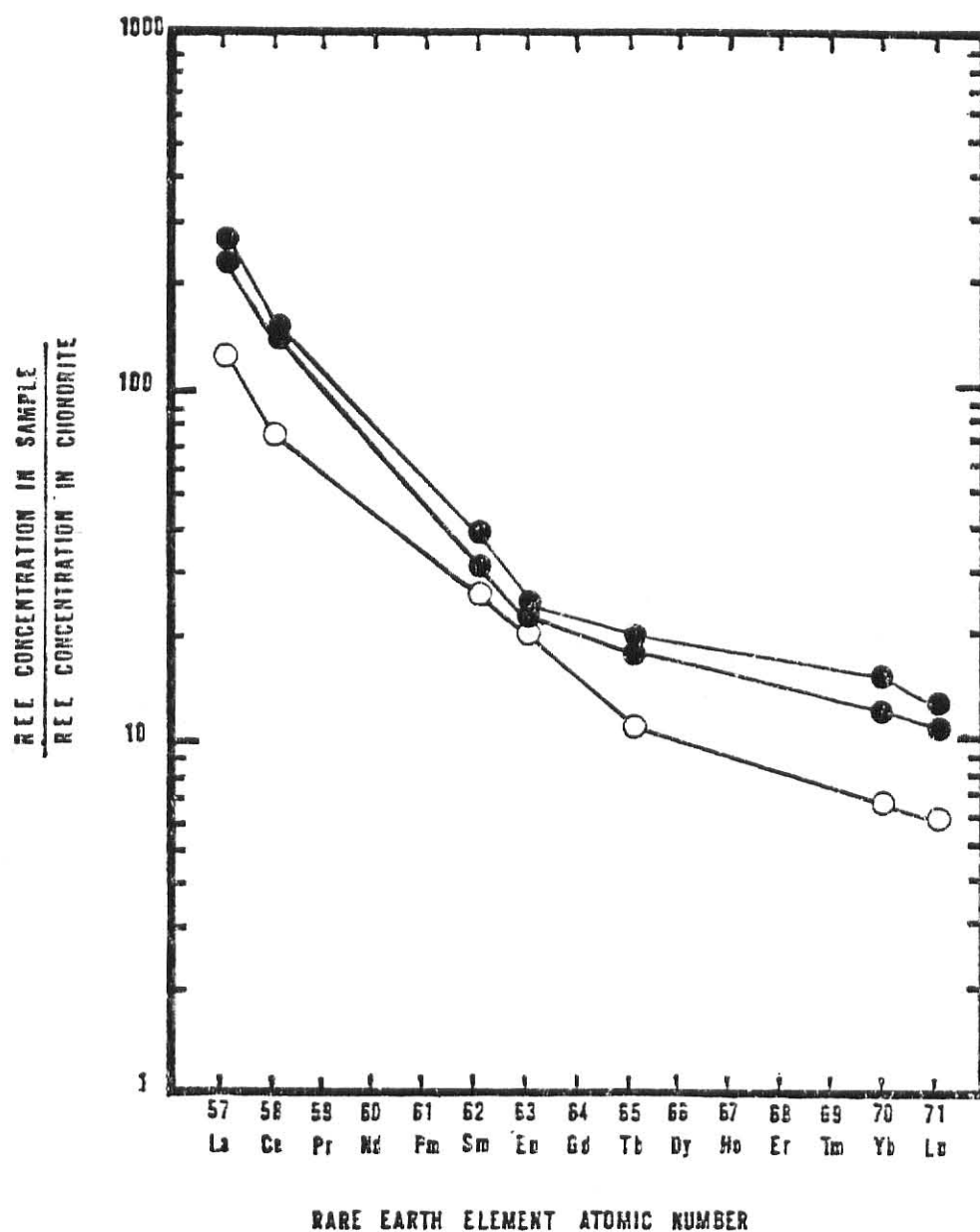


FIGURE 12c: Chondrite-normalized REE distributions of:
 LATITE (●) samples RH-43 and RH-47
 RHYODACITE (○) sample RH-5

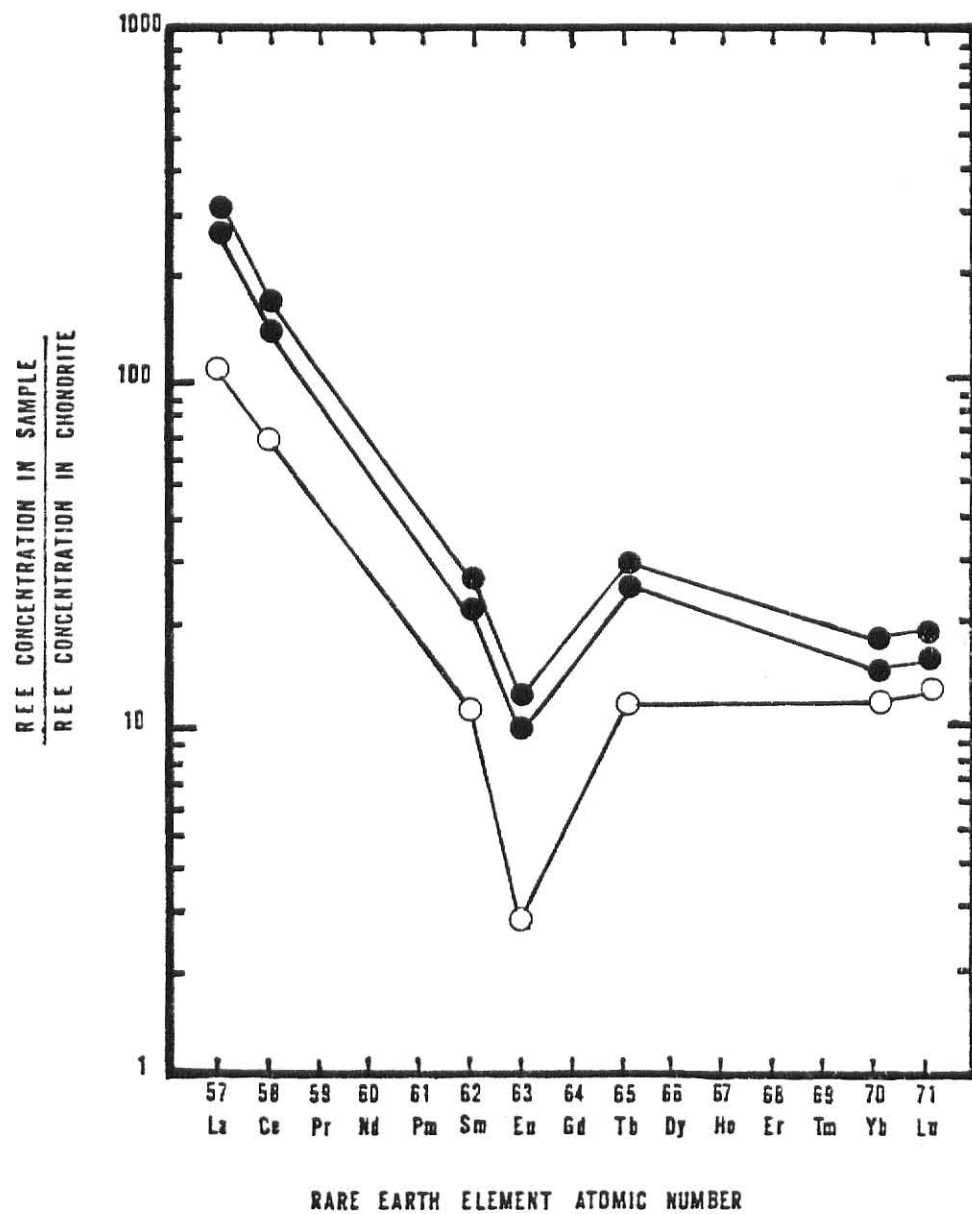


FIGURE 12d: Chondrite-normalized REE distributions of:
 TRACHYTE (●) samples RH-7 and RH-42
 RHYOLITE (○) sample RH-4

Strontium-Isotope Ratios

$^{87}\text{Sr}/^{86}\text{Sr}$ ratios were measured in representative samples from the trachyandesite unit (Tb, RH-39), the latite unit (Tp, RH-43), and the rhyolite unit (Trr, RH-4). Initial $^{87}\text{Sr}/^{86}\text{Sr}$ ratios were calculated from the measured ratios using the relationship:

$$(^{87}\text{Sr}/^{86}\text{Sr})_I = (^{87}\text{Sr}/^{86}\text{Sr})_M - (^{87}\text{Rb}/^{86}\text{Sr})(e^{\lambda t} - 1)$$

where:

$(^{87}\text{Sr}/^{86}\text{Sr})_I$ = initial ratio

$(^{87}\text{Sr}/^{86}\text{Sr})_M$ = present ratio

λ = ^{87}Rb decay constant

$(1.42 \times 10^{-11} \text{y}^{-1})$

t = time since solidification

(assumed to be 30 million years)

The values obtained are listed in Table 7 below.

Table 7: Sr-isotope data for samples from the Rosita Hills suite

Sample Number	Rock Unit	Rock Name	$(^{87}\text{Rb}/^{86}\text{Sr})$	$(^{87}\text{Sr}/^{86}\text{Sr})_M$	$(^{87}\text{Sr}/^{86}\text{Sr})_I$
RH-4	Trr	rhyolite	13.28	0.7129	0.7072
RH-43	Tp	latite	0.41	0.7076	0.7074
RH-39	Tb	trachy-andesite	0.26	0.7058	0.7057

Petrography

Standard petrographic thin sections were prepared from each rock specimen analyzed chemically. Modal compositions and mineral relations were determined from these thin sections. Petrographic descriptions are provided in Appendix I and a summary of mineralogical and textural features of the samples is provided in Table 8.

There is a considerable degree of similarity among the textural characteristics of the various rock types of the suite. Most of the samples examined contained numerous phenocrysts in a cryptofelsic groundmass. Phenocryst content among the samples ranges typically from about 30 to 65 percent of the total volume. The rhyolite (Trr) sample, however, has very few phenocrysts (less than 3 percent). One of the syenodiorite (Tbs) samples has hypidiomorphic-granular texture.

Plagioclase is the predominant phenocryst in the syenodiorite (Tbs), trachyandesite (Tb), rhyodacite (Tbm), and latite (Tp) samples. Sanidine-anorthoclase is the predominant phenocryst in the trachyte (Tt) and rhyolite (Trr) samples. The proportion of sanidine-anorthoclase tends to increase among the intermediate rock types corresponding to increasing SiO_2 . Predominant mafic phenocrysts vary from clinopyroxene in the syenodiorite (Tbs) samples, to hornblende in the trachyandesite (Tb) and rhyodacite (Tbm) samples, to biotite in the latite (Tp) and trachyte (Tt) samples.

TABLE 8: Petrographic summary of rock samples analyzed in this study

Sample Number	Lithologic Unit	Rock Name	Texture	Mineralogy
RH-49	Tl	OLIVINE VOGESITE	porphyritic, panidiomorphic	<u>phenocrysts:</u> olivine, plagioclase <u>groundmass:</u> plagioclase, clino- pyroxene, amphibole, black oxides, glass
RH-22	Tbs	SYENODIORITE	hypidiomorphic- granular	plagioclase (An 30), orthoclase, clinopyroxene, biotite, black oxides, nepheline
RH-23	Tbs	PYROXENE ANDESITE	porphyritic, cryptofelsic groundmass	<u>phenocrysts:</u> plagioclase (An 30), orthoclase, clino- pyroxene <u>groundmass:</u> black oxides, glass, cryptofelsic material
RH-39	Tb	TRACHYANDESITE	porphyritic, cryptofelsic groundmass	<u>phenocrysts:</u> plagioclase (An 20), clinopyroxene, san- idine-anorthoclase, biotite, hornblende (apatite inclusions) <u>groundmass:</u> cryptofelsic material, black oxides, glass

TABLE 8: Petrographic summary of rock samples analyzed in this study

Sample Number	Lithologic Unit	Rock Name	Texture	Mineralogy
RH-27	Tb	TRACHY-ANDESITE	porphyritic, cryptofelsic groundmass	<u>phenocrysts:</u> plagioclase (An 18), sanidine-anorthoclase hornblende (apatite inclusions), biotite clinopyroxene <u>groundmass:</u> cryptofelsic material, black oxides, glass
RH-43	Tp	LATITE	porphyritic, cryptofelsic groundmass	<u>phenocrysts:</u> plagioclase (An 12), sanidine-anorthoclase hornblende, biotite <u>groundmass:</u> cryptofelsic material, quartz, black oxides, glass
RH-47	Tp	LATITE	porphyritic, cryptofelsic groundmass	<u>phenocrysts:</u> plagioclase (An 12), sanidine-anorthoclase hornblende, biotite <u>groundmass:</u> cryptofelsic material, quartz, black oxides, glass
RH-5	Tbm	RHYO-DACITE	microporphyrritic, cryptofelsic groundmass	<u>phenocrysts:</u> plagioclase (An 15), hornblende, biotite, sanidine-anorthoclase <u>groundmass:</u> cryptofelsic material, quartz, black oxides

TABLE 8: Petrographic summary of rock samples analyzed in this study

Sample Number	Lithologic Unit	Rock Name	Texture	Mineralogy
RH-7	Tt	TRACHYTE	pilotaxitic, orthophyritic, porphyritic	<u>phenocrysts:</u> sanidine-anorthoclase, plagioclase (An 10), biotite <u>groundmass:</u> sanidine, plagioclase, quartz
RH-8	Tt	TRACHYTE	porphyritic, cryptofelsic groundmass	<u>phenocrysts:</u> sanidine-anorthoclase, plagioclase (An 10), biotite <u>groundmass:</u> cryptofelsic material
RH-42	Tt	TRACHYTE	porphyritic, cryptofelsic groundmass	<u>phenocrysts:</u> sanidine-anorthoclase, plagioclase (An 10), hornblende <u>groundmass:</u> cryptofelsic material
RH-4	Trr	RHYOLITE	flow-banded glass, slightly porphyritic	<u>phenocrysts:</u> sanidine

DISCUSSION

Evidence of Fractional Crystallization

Many similarities in mineralogy and chemical composition exist among the various volcanic rock units within the Rosita Hills district. These similarities have led previous investigators to conclude that the different types of magma extruded within the district were derived through fractionation of a common homogeneous parent material. For example, Cross (1896) observed:

" . . . the various magmas erupted from the Rosita volcano are such as might be expected under the current theory regarding the origin of magmas by differentiation of a nearly homogeneous source. The series is not complete, but there is nothing in this fact necessarily antagonistic to the theory . . .

. . . The variations in the series are thought to have arisen through chemical and physical agencies, resulting in a relative concentration of the several chemical elements in different parts of the original molten mass. The process is called differentiation, and while laws operating to produce it are as yet very imperfectly understood, it is clear that either differentiation in this broad sense is a fact or the part of the earth's interior from which the magmas come has always been heterogeneous."

Siems (1968) considered the suite to represent the liquid line of descent of a parent magma as the result of crystal fractionation. He suggested that the parent magma was probably of trachyandesitic composition and derived through anatexis of crustal rocks. He noted that fractionation might occur as the result of either compositional layering within a magma chamber or progressive differential fusion.

The smooth trends of many of the major and trace-element variation diagrams tend to support the idea that some magmas of the Rosita Hills might have been derived by fractional crystallization of a homogenous parent magma. If a parent magma of andesitic composition were to occupy some sort of magmatic chamber at shallow depths (less than 30 km) and slowly crystallize, it could conceivably undergo chemical fractionation to produce these trends. As suggested by Bowen (1928), removal of the early formed crystalline phases such as plagioclase and clinopyroxene by processes such as gravity settling and filter pressing would cause the residual liquid to become depleted in compatible elements such as Fe, Ca, and Mg while undergoing a corresponding increase in SiO_2 content.

Some of the aspects of the Rosita Hills suite which support such a model include the following:

- (1) The concentrations of Fe, Ca, Mg, and Sr systematically decrease with increasing SiO_2 content among the samples analyzed with relatively few exceptions. This compositional trend would be expected in the residual magmatic liquids from which plagioclase, clinopyroxene, hornblende, and magnetite were being extracted. The occurrence of these minerals as phenocrysts in many of the samples indicates that the minerals crystallized at depth prior to eruption (Table 6).
- (2) The concentrations of K and Rb among samples gradually increase corresponding to increasing SiO_2 content. This might also be the expected liquidus trend because these elements

tend to be rejected by the early formed crystallizing phases mentioned above.

(3) The smooth trends on the alkali-iron-magnesium triangular variation diagram (Figure 6) and the Na_2O - K_2O - CaO variation diagram (Figure 7) follow the liquid path observed during the crystallization of an andesitic liquid in the experiments of Green and Ringwood (1968).

(4) Comparison of the chondrite-normalized REE distributions of trachyandesite (Tb), latite (Tp), trachyte (Tt), and rhyolite (Trr) illustrates the development of an increasingly negative Eu anomaly which would be expected in a magma from which plagioclase was being extracted.

(5) Systematic gradational changes can be observed in the phenocryst mineralogy of the samples corresponding to increasing silica content. There is a general trend toward decreasing proportions of plagioclase and clinopyroxene and increasing proportions of potassium feldspar and biotite corresponding to increasing silica content.

(6) A crystallization trend of decreasing K/Rb with increasing K_2O can be seen in the trachyandesite (Tb)-latite (Tp)-trachyte (Tt) sequence (Figure 10).

Other chemical and mineralogical characteristics argue against a simple case of fractional crystallization of a single homogeneous parent as a mechanism through which the compositional diversity of the suite could have originated. These characteristics include the following:

- (1) The K/Rb ratios among samples of the suite are considerably varied. The K/Rb ratios of the rhyolite (Trr), rhyodacite (Tbm), and lamprophyre (Tl) plot away from the main trend of the suite on the K/Rb vs. K_2O graph (Figure 10).
- (2) Different degrees of REE fractionation occur within the rock types and analyzed. Most of the samples analyzed have La/Lu ratios between 18 and 24. The lamprophyre (Tl), however, is significantly more fractionated (La/Lu = 30) while the rhyolite (Trr) is much less fractionated (La/Lu = 8).
- (3) Differences also occur in the degree of REE enrichment among the various rock types analyzed. REE values for the rhyodacite (Tbm) and rhyolite (Trr) samples are considerably lower than the rest of the suite.
- (4) Major-element variations can be correlated with SiO_2 content but the degree of silica enrichment does not consistently correlate with the chronological sequence of eruptive events. For example, the rhyolite (Trr) erupted prior to much less fractionated rock types such as the trachyandesite (Tb), syenodiorite (Tbs), and latite (Tp). Similarly, the lamprophyre (Tl) is apparently a late-stage intrusive despite the fact that it is the most basic rock type within the suite.

These factors suggest that if fractional crystallization was the mechanism responsible for chemical and mineralogical variations within the suite, then there must have been more than one cycle of the process involved. It is possible that the rhyodacite (Tbm) and rhyolite (Trr) represent derivatives of one parent magma during the early stages of eruption within

the province. Subsequent fractional crystallization of a separate but genetically related magma might have produced the trachyandesite (Tb)-latite (Tp)-trachyte (Tt) sequence. The lamprophyre (Tl) dikes indicate the existence of a third distinct magma body.

Theories Concerning the Origin of Alkali-Calcic Magmas

Several mechanisms have been proposed to explain the origin of alkali-calcic volcanic suites. These have been reviewed by Boettcher (1973), Green and Ringwood (1968), Zielinski and Lipman (1976), and Ringwood (1974). The most reasonable of these petrogenic models include the following:

(1) Alkali-calcic magmas of intermediate composition could be derived through direct partial melting of an upper-mantle peridotite source which was enriched in the large-ion lithophile elements. Kushiro et al. (1972) provided experimental data which indicated that silica-rich melts of roughly rhyodacite composition coexisted with olivine, clinopyroxene, and orthopyroxene during the fusion of a xenolithic lherzolite nodule under conditions of high water pressure ($P_{H_2O} = 26 \text{ kb}$) and high temperatures (1190°C). The experiments of Mysen and Boettcher (1975) indicated that andesitic liquids might form by anatexis of hydrous mantle peridotite over a broad range of temperatures.

Other experimental groups, however, have suggested that these conclusions were based on an incorrect assessment of

the quench products of the experiments. Nicholls and Ringwood (1973) and Green (1973) attributed the high-silica nature of the quench products to formation of metastable mineral phases during cooling. Green (1973) and Ringwood (1974) provided experimental evidence that indicated that either olivine-tholeiite basalt or quartz-tholeiite basalt resulted from hydrous partial melting of peridotite.

(2) Intermediate alkali-calcic magmas could be produced by fractional crystallization of a basaltic magma as suggested by Bowen (1928). Experimental work of Green (1971) showed that it is possible to produce tholeiitic basalt through partial melting of mantle pyrolite at depths between 70 and 100 km. Upon rising toward the surface, the load pressure and water pressure are reduced causing the olivine solidus temperature to rise as shown by Nicholls and Ringwood (1973). As a result, olivine will crystallize at depths of about 30 km or less even if the temperature is held constant. Nicholls and Ringwood (1973) estimated that a basaltic andesite or possibly andesite with a maximum SiO_2 content of about 58 percent could result from the crystallization and removal of olivine and spinel from a tholeiitic magma.

Green and Ringwood (1968) demonstrated that andesite and dacite could be produced by crystallization of pyroxene and low-silica amphibole from a basalt under conditions of high water pressure. Their experiments indicated that crystallization of these minerals would result in the so-

called calc-alkaline trend on AFM diagrams (such as Figure 6) in which no enrichment occurs in Fe relative to Mg in the residual liquid. Crystallization of olivine and pyroxene without amphibole on the other hand, would result in a marked increase in the Fe/Mg ratio of the residual liquid producing the so-called tholeiitic trend on AFM diagrams. This effect, however, might be offset by crystallization of magnetite.

(3) Assimilation of upper crustal material by a basaltic magma formed at greater depth could result in a magma with alkali-calcic chemical characteristics (Bowen, 1928). The mechanism might involve the melting of wall rocks and xenolithic material or possibly the mixing of basaltic magmas with melts formed at shallow depths.

(4) Intermediate alkali-calcic magmas could result from the partial melting of quartz eclogite derived from the transformation of oceanic basaltic crust within a subduction zone as suggested by Green and Ringwood (1968). Experimental data by Hill and Boettcher (1970) indicate that during subduction oceanic crust (consisting largely of basalt, gabbro, and greenschist) is first transformed to an amphibolite facies, and at depths greater than 100 km the amphibolite is transformed to quartz eclogite, provided temperatures do not exceed the melting temperature of amphibolite. Thermal models of Oxburgh and Turcotte (1970) indicate that conditions along the Benioff zone at depths less than 100 km are subsolidus for amphibolite.

Experimental results of Green and Ringwood (1968) indicate that partial melting of eclogite under dry conditions is capable of producing andesitic or basaltic-andesitic melts, whereas partial melting of the same source material under hydrous conditions could result in more silicic melts of rhyodacite composition. Ringwood (1974) estimated that conditions of eclogite melting in a subduction system would occur between 100 and 150 km depth if temperatures exceeded 750°C.

(5) Ringwood (1974) suggested that andesite might form by partial melting of subducted quartz eclogite oceanic crust followed by reaction of the resulting liquid with overlying mantle pyrolite. Such a reaction would produce a garnet pyroxenite with a density lower than surrounding pyrolite. Diapirs of this garnet pyroxenite would theoretically become detached from the Benioff zone and rise upward, while undergoing partial melting in the process. Liquids resulting from this two-stage process would be enriched in silica and large-ion lithophile elements and would have strongly fractionated REE patterns.

(6) Brooks et al. (1976) suggested that many continental andesitic volcanic suites may represent partial melting of lower lithospheric material which has fractionated from the asthenosphere through geologic time and has slowly accreted below the continental masses. Such material would likely have a major-element composition similar to basalt and would be enriched in Rb, REE, and other large ion lithophile elements

relative to the asthenosphere. They suggested that pseudo-isochrons of initial $^{87}\text{Sr}/^{86}\text{Sr}$ ratios in numerous continental andesitic volcanic suites reflect the heterogeneity in age and enrichment of the lower lithosphere. Melting of these materials (primarily eclogite) could result from processes related to subduction or through thermal perturbations in the underlying asthenosphere or mesosphere.

Trace-Element Modeling

Trace-element concentrations can be used to place certain constraints on the possible petrogenic models considered. These elements are preferentially partitioned between crystalline solids and coexisting liquids in silicate systems under equilibrium conditions. Such partitioning is to some degree thermodynamically predictable, and a number of mathematical relationships have been proposed (e.g., Gast, 1968; Shaw, 1970; Hertogen and Gijbels, 1976) to model the expected trace-element concentrations in a liquid derived by partial fusion of a multiple-phase source rock. These models utilize published partition coefficients (Appendix III), which are primarily obtained through measurement of trace-element concentrations in coexisting phenocryst and groundmass assemblages representing equilibrium conditions.

Uncertainties concerning the conditions of melting at great depths within the earth limit the exactness of this approach to modeling the origin of magma. In order to

utilize the models, the following estimations and assumptions must be made:

- (1) The mineralogy and phase proportions of the various types of possible source rocks must be estimated.
- (2) Different phases of the source rock do not melt at the same rate or temperature. The relative contribution of each solid phase to the melt must therefore be estimated.
- (3) The manner in which the resulting melt is removed from the source area must be assumed (i.e.: whether or not the melt remains in equilibrium contact with the source rock or continually or intermittently migrates away from the source region during progressive melting).
- (4) The concentrations of trace elements within the source rock must be estimated.
- (5) The partition coefficients must be estimated. Partition coefficients have been shown to be both temperature-and composition-dependent, and the values commonly used represent average values.

Despite these limitations, trace-element modeling provides a semi-quantitative means of eliminating certain hypotheses concerning the origin and evolution of magma. While not providing a unique answer to the question of petrogenesis, trace-element modeling can limit the range of possible source materials and impose constraints on the types of chemical changes that would be expected to occur as the result of fractional crystallization.

Modeling of Fractional Crystallization Trends

Trace-element modeling can be used to evaluate the extent to which fractional crystallization was operative in producing the chemical variations of the suite. Modeling can verify the direct genetic linkages among magma types representing differentiated liquids derived from a common parent magma. The mathematical relationship of Haskin et al. (1970) in Appendix III provides a good approximation of the relative degrees of enrichment or depletion of a given trace element as the result of crystallization and removal of a particular mineral phase. Table 9 summarizes the independent effects of the extraction of common rock-forming minerals as predicted using that formula, together with well-tested partition coefficients obtained from the literature and compiled in Appendix III.

As summarized in Table 9, concentrations of REE in a magma would be expected to increase as the result of extraction of olivine, spinel and biotite. Crystallization and removal of hornblende and apatite, on the other hand, could cause significant depletion of REE in silica-rich magma. Plagioclase and K-feldspar incorporate Eu^{2+} preferentially to other REE (which exist in 3+ ionic states), and extraction of these mineral phases therefore leads to the development of a negative Eu anomaly in the REE distribution of the residual liquid. Clinopyroxene has a slight preference for heavy REE (Yb, Lu) relative to light REE (La, Ce). Extraction

of clinopyroxene in large amounts could deplete heavy REE relative to light REE, thereby changing the La/Lu ratio.

TABLE 9: Changes in concentrations of trace elements in magma due to extraction of various mineral phases.

	REE					Ba	Sr	Rb
	Ce	Sm	Eu	Dy	Yb			
OLIVINE (x)	+	+	+	+	+	+	+	+
SPINEL (x)	+	+	+	+	+	+	+	+
CLINOPYROXENE (*)	+	-	-	-	-	+	+	+
PLAGIOCLASE (*)	+	+	-	+	+	+	-	+
HORNBLende (*)	-	-	-	-	-	+	+	+
K-FELDSPAR (*)	+	+	-	+	+	-	-	+
BIOTITE (*)	+	+	+	+	+	-	+	-
APATITE (*)	-	-	-	-	-			

(+) enrichment of trace element in magma

(-) depletion of trace element in magma

based on trace element modeling equation of Haskin et al. (1970; Appendix III) and partition coefficients listed in Tables 17 and 18

(x) basaltic magma (*) intermediate to rhyolitic magma

Most minerals which crystallize in magmas of basaltic or intermediate composition tend to reject Rb and Ba from their crystal structure, and therefore concentrations of Rb and Ba are enriched in the residual liquid. Biotite and K-feldspar, however, are exceptions in that both incorporate significant amounts of Ba, and extraction of these minerals can lead to lower concentrations of Ba in the liquid. Biotite will also incorporate Rb to a small degree, but the effect is minimal in altering the Rb concentration in the liquid. Plagioclase and K-feldspar incorporate Sr readily, and extraction of these phases can cause significant depletion of Sr in residual liquids. Other minerals such as olivine, clinopyroxene, spinel, biotite, and hornblende tend to reject Sr from their crystal structures.

If two or more of the rock types within the Rosita Hills suite are related to one another such that they represent fractional crystallization derivatives of a common parent magma, then one should be able to explain the changes in concentrations of trace elements in terms of extraction of specific minerals.

Relationship Between Rhyodacite (Tbm) and Rhyolite (Trr)

Many chemical relationships between the rhyodacite (Tbm) and the rhyolite (Trr) suggest that these two units might be related by fractional crystallization of a common parent magma. Together, they appear to form trends on major-element variation diagrams. On several such diagrams

(such as Figures 4a, 5a, 9 and 10), the variation trend of the two compositions appears distinct from the rest of the suite.

Field investigations of Siems (1968) and Sharp (1978) indicated that the extrusion of the rhyolite (Trr) closely followed that of rhyodacite (Tbm). The total amount of rhyolitic material extruded at that time was volumetrically much larger than the rhyodacite body (Siems, 1968).

For most elements considered, the transition from the rhyodacite composition to the rhyolite composition can be explained in terms of fractionation by extraction of plagioclase, K-feldspar, and biotite. These minerals would account for the depletion of Sr and Ba and the enrichment of Rb in the rhyolite relative to the rhyodacite. Crystallization of the feldspars would produce the negative Eu anomaly that is present in the rhyolite but absent in the rhyodacite.

Difficulties in this suggested transition arise in the fact that the REE distributions of the two rock types have different degrees of La/Lu fractionation. The light REE concentration in the rhyodacite sample is greater than that of the rhyolite, whereas the heavy REE content of the rhyodacite is lower than that of the rhyolite. A fractional crystallization model that would cause an increase in the heavy REE concurrent with a decrease in the light REE, as a result of extraction of some combination of the minerals listed in Table 9, is not possible. Such phenomena would require a separating phase that had a partition coefficient that was high for the light REE and low for the heavy REE. Table 9, however, does not

account for all possible minerals nor does it take into account other phase relationships such as might exist between magmatic liquids and associated vapors.

Differences in REE fractionation between the rhyolite and rhyodacite are much more easily explained in terms of garnet fractionation during partial melting. Garnet in the source material will retain heavy REE, and the degree to which garnet melts affects the heavy REE content of the resulting liquid.

The many similarities between the rhyolite and rhyodacite suggest that they were derived from very similar sources. The absence of an Eu anomaly in the REE distribution of the rhyodacite suggests that it is a primary magma which has not been significantly altered by low-pressure crystallization of feldspars. The low concentrations of the heavy REE in the rhyodacite, however, might be indicative of high-pressure crystallization of clinopyroxene or possibly garnet.

The rhyolite, on the other hand, appears to have undergone considerable feldspar fractionation as indicated by its negative Eu anomaly. The magma from which it evolved was probably very similar in many respects to the rhyodacite and was probably derived from the same source regime.

Relationship Between Trachyandesite (Tb) and Latite (Tp)

A similar genetic linkage is apparent between the trachyandesite (Tb) and latite (Tp). These two rocks are very similar to one another in terms of petrography and

chemical composition. Siems (1968) and Sharp (1978) determined that the intrusion of the latite (Tp) stock occurred subsequent to the emplacement of the trachyandesite (Tb) body. The volume of the two units is approximately equal. It seems possible that the latite magma represented a liquid differentiate of the trachyandesite by fractional crystallization.

Trace-element modeling was used to test this possibility. It was found that the change in concentrations of REE, Ba, Rb, and Sr between trachyandesite sample RH-39 and latite sample RH-43 could have been caused by crystallization and extraction of approximately 15% plagioclase, 5% hornblende, and 7% K-feldspar from the trachyandesite. Minor amounts of biotite and clinopyroxene would also be permissible in this model, with little change in the net result. Plagioclase, K-feldspar, hornblende, and biotite occur as phenocrysts in both rock units.

Relationship of Trachyte (Tt) to Other Rock Units

The trachyte (Tt) is similar in many respects to the trachyandesite (Tb) and latite (Tp). The trachyte was extruded after the emplacement of the latite stock (Siems, 1968). The higher silica content of the trachyte suggests that it might represent a further differentiate of the trachyandesite-latite liquidus trend discussed above.

Problems arise in attempting to explain differences in concentrations of some trace elements between latite and

trachyte samples. Trachyte samples contain less than half as much Ba as the latite samples whereas concentrations of Rb are larger in trachyte samples than in latite samples. Decreases in Ba in residual liquids could be attributed to either biotite or K-feldspar crystallization. Significant biotite extraction, however, would result in a depletion of Rb in the liquid instead of enrichment of Rb. Significant K-feldspar crystallization would not be a likely explanation for the depletion of Ba in trachyte relative to latite, because trachyte samples have nearly twice as much K_2O as the latite samples. These factors suggest that the trachyte composition does not represent a direct differentiate of the latite magma.

Relationship Between Syenodiorite (Tbs) and Trachyandesite (Tb)

Sharp (1978) classified the syenodiorite (Tbs) as a late-stage intrusive phase of the trachyandesite (Tb) unit. The syenodiorite intrusion is small in volume compared to the trachyandesite and was emplaced after the trachyandesite (Siems, 1968). The syenodiorite is similar in some respects to the trachyandesite in terms of major-element and trace-element composition.

It seems unlikely, however, that the syenodiorite magma could have evolved from the trachyandesite magma. The syenodiorite is significantly undersaturated with silica whereas the trachyandesite samples are saturated with silica. Furthermore, the syenodiorite contains much more CaO and Fe_2O_3 than the trachyandesite, whereas this is opposite of what would be expected in an evolving residual liquid. It might be

suggested that the syenodiorite represents a cumulative variety of the trachyandesite, but significant accumulation of plagioclase should be reflected in a positive Eu anomaly. No such anomaly is observed in the REE pattern of the syenodiorite.

Relationship Between Syenodiorite (Tbs) and Lamprophyre (Tl)

The syenodiorite composition might possibly represent a differentiate of the lamprophyre (Tl). The volume of both rock units is small compared to other rock types in the Rosita Hills suite. The chronological relationship between the two units is not clear from field evidence. The absence of a negative Eu anomaly in the REE distribution of the syenodiorite suggests that it has not been extensively modified by plagioclase crystallization. Extraction of a combination of olivine, clinopyroxene, and magnetite, however, could conceivably produce a liquidus transition from the lamprophyre to the syenodiorite. Such a transition is consistent with available trace-element data.

Thus, trace-element modeling places some restrictions on the degree to which the various magma types of the Rosita Hills suite were related to one another by fractional crystallization processes. At the same time, however, the chemical similarities among the various magma types, the manner in which their compositions are gradational to one another, and their spatial and chronologic proximity suggest that they must have close genetic relationships. It is therefore

suggested that the magma types represented in the Rosita Hills suite originated from a common source which, for a period of time, intermittantly generated liquids of varied composition through partial melting. Many of the variations within the suite probably represent some heterogeneity in the composition of the source material. The variations could also represent different percentages of melting or varying H_2O pressure. Ample evidence does exist, however, that suggests that low-pressure fractional crystallization in shallow magma chambers has modified the more siliceous members of the Rosita Hills suite.

Modeling of Possible Source Materials

Trace-element models allow for a limited range of source materials capable of generating the observed REE distributions. All of the rock types analyzed have REE patterns that are significantly enriched in the light REE (La, Ce) compared to the heavy REE (Yb, Lu). This phenomenon is generally attributed to the presence of garnet in the residual material during partial melting (Zielinski and Lipman, 1976). Figure 13, for example, illustrates the effect of 1 to 30 percent partial melting of an REE-enriched eclogite. In this case, the concentrations of the light REE in the resulting melt are considerably greater than the concentrations in the original source material. The heavy REE, on the other hand, are depleted in the melt with respect to the source.

The degree of enrichment of light REE with respect to heavy REE is a function of the proportion of garnet in the

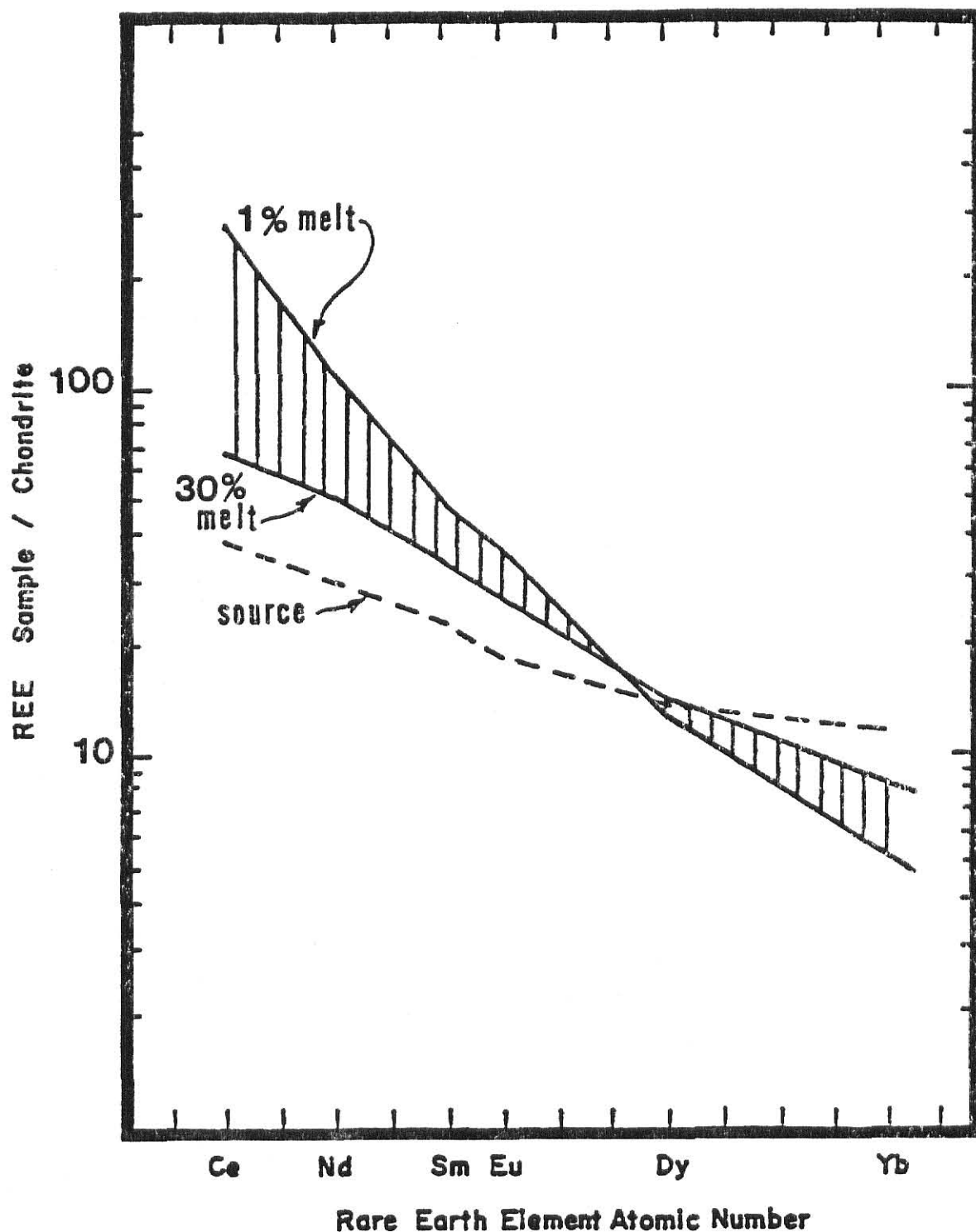


FIGURE 13 : Predicted range of REE concentrations produced by 1 to 30 percent melting of an eclogite source with initial mineral ratio of clinopyroxene/garnet = .85/.15, which melts in a ratio of clinopyroxene/garnet = .75/.25 .

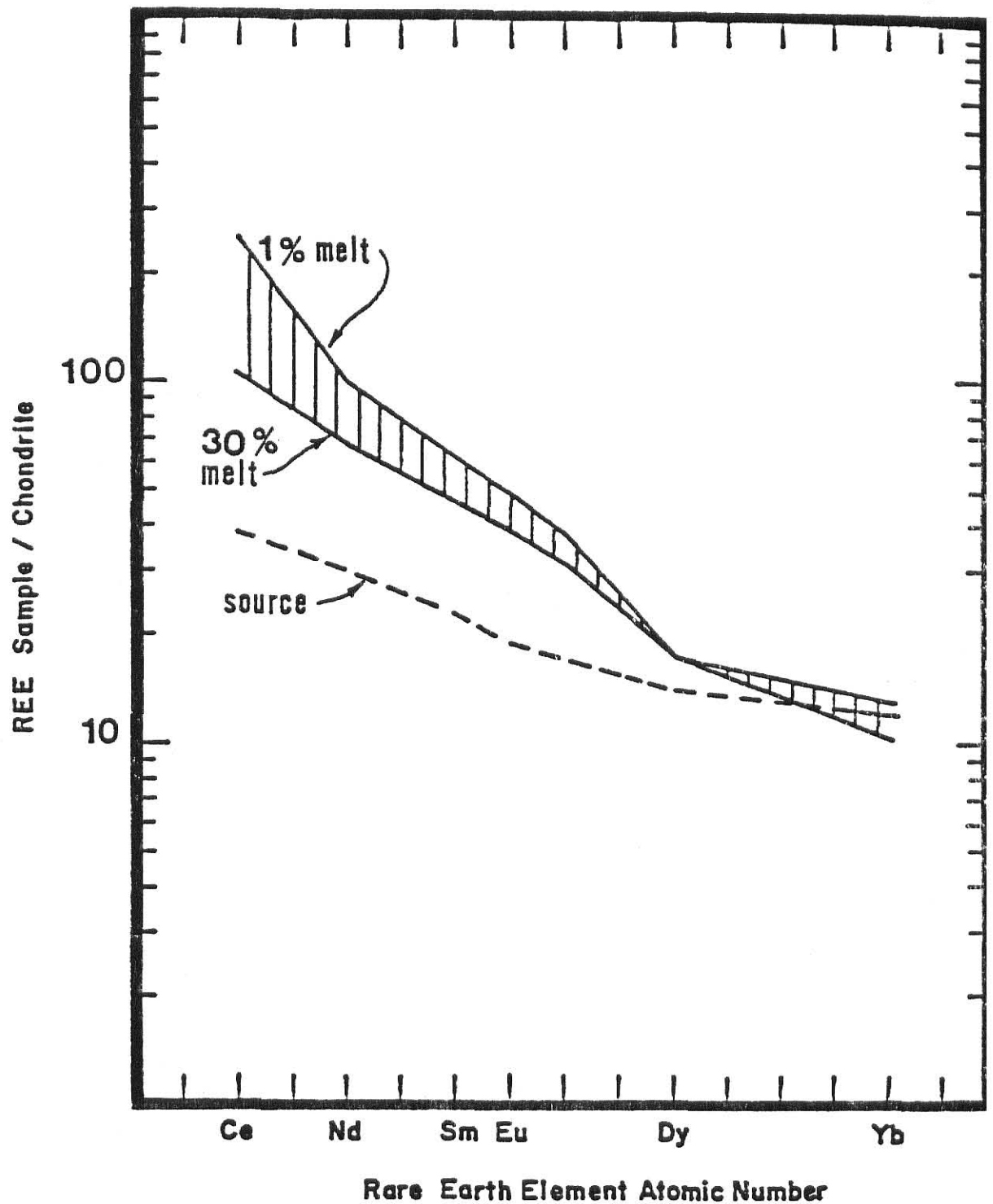


FIGURE 14 : Predicted range of REE concentrations produced by 1 to 30 percent melting of an eclogite source with an initial mineral ratio of clinopyroxene/garnet = .95/.05, which melts in a ratio of clinopyroxene/garnet = .75/.25 .

TABLE 10 Comparison of REE concentrations (ppm) in model sources with typical REE concentrations in basalt and peridotite

	model eclogite source (Figures 13 and 14)	oceanic ridge basalt (a)	continental basalt (b)	model peridotite source (Figure 15)	ultra- mafic nodules (c)
La	13.5	11.2	31.9	2.7	1.6
Ce	32.8	24.3	59.0	7.1	1.9
Nd	17.4	11.9	33.9	4.6	0.7
Sm	4.8	3.1	6.6	1.6	0.2
Eu	1.5	1.0	1.9	0.5	0.1
Tb	0.8	0.7	1.0	0.4	0.03
Yb	2.1	2.1	2.6	0.9	0.2
Lu	0.3	0.3	0.4	0.2	0.1

(a) Average of analyses of 10 tholeiitic basalt samples from the Mid-Atlantic Ridge at 43°N (Shibata et al., 1979)

(b) Average of analyses of 282 continental basalt samples from North America, Africa, India, and Asia (Frey et al., 1968)

(c) Average of analyses of 3 ultramafic xenoliths (lherzolite nodule from Dreiser Weiher, Germany; dunite nodule from Mt. Leura, Australia, garnet peridotite nodule from Kakanui, New Zealand), Frey et al., (1971)

source material, the relative rate at which garnet melts with respect to the other phases, and the degree of partial melting that occurs. Figure 14 illustrates how changing the proportion of garnet in the source material affects the resulting REE enrichment. The original REE concentration in the source and the percentage of melting illustrated in Figure 14 are the same as those shown in Figure 13.

Table 9 compares the REE-source concentrations used in these models with those of samples of oceanic ridge and continental basalt. The values listed for oceanic basalt are among the highest found in the literature for samples from that tectonic environment. Values for oceanic tholeiitic basalt are typically much less enriched in the light REE (La, Ce).

Figure 15 illustrates how a smaller degree of melting of a garnet peridotite could also generate the REE distributions observed in trachyandesite (Tb), syenodiorite (Tbs), and lamprophyre (Tl). This model allows for up to 10 percent partial melting but requires a peridotite source that is enriched in REE relative to estimates of average REE concentrations in the upper mantle (see Table 9).

Initial $^{87}\text{Sr}/^{86}\text{Sr}$ ratios for trachyandesite (Tb), latite (Tb), and rhyolite (Trr) range from 0.7057 to 0.7074. These are probably too high for the magmas to be considered as direct partial melts of mantle material. Basaltic material fractionated from the mantle early in the history of the earth, however, could have been enriched in Rb as suggested by Brooks et al. (1976). Melts derived from such material

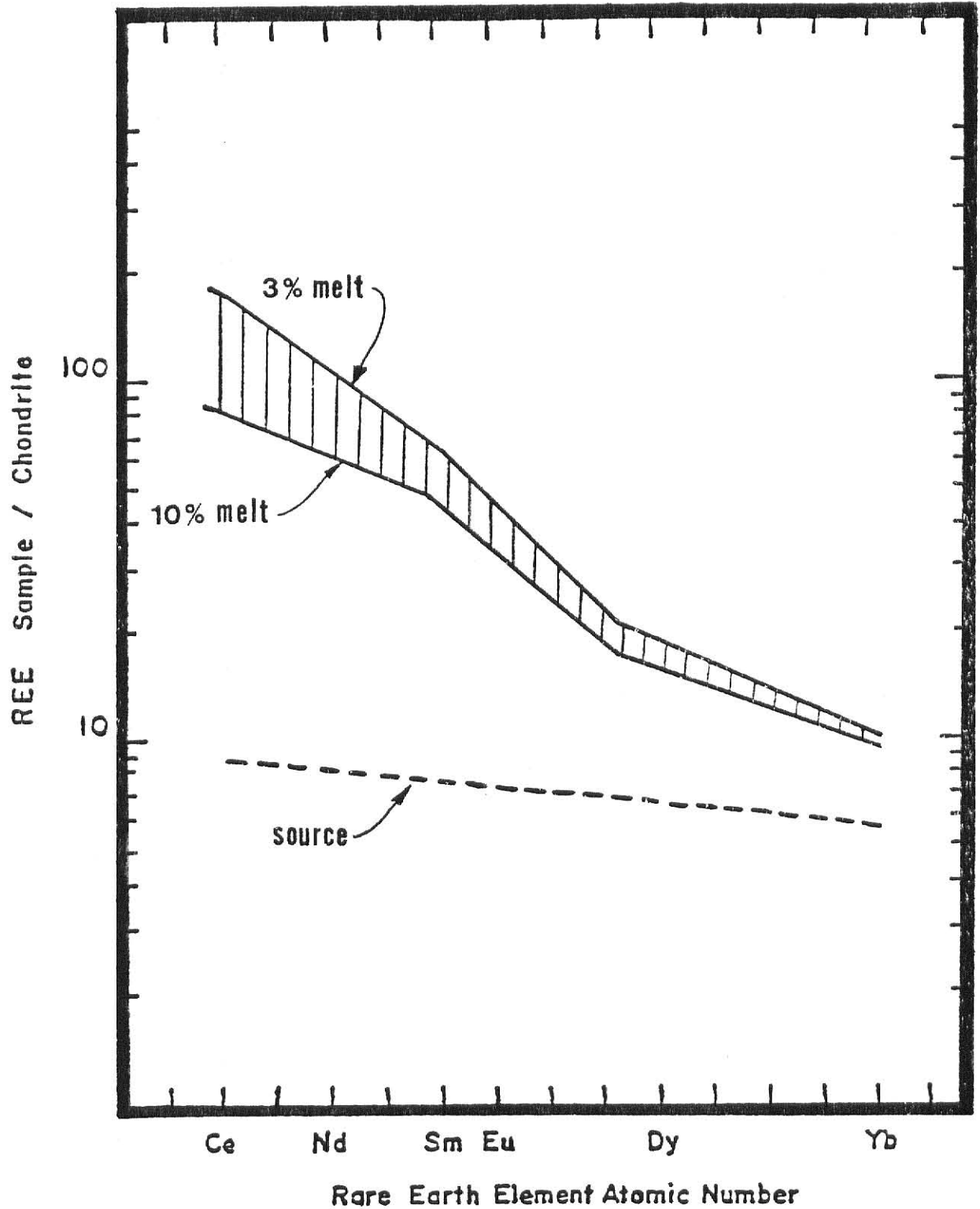


FIGURE 15: Predicted range of REE concentrations in magma produced by 3 to 10 percent melting of a peridotite with an initial mineral ratio of olivine/clinopyroxene/orthopyroxene/garnet = .60/.13/.25/.02 melting in a ratio of .42/.30/.18/.10 (after Cullers and Arnold, 1980)

might have initial $^{87}\text{Sr}/^{86}\text{Sr}$ ratios similar to those observed in the Rosita Hills suite.

A reasonable source material for the intermediate magma types of the suite (trachyandesite, rhyodacite, and latite) would be lower lithospheric eclogite. Such eclogite could conceivably represent basaltic derivatives that were fractionated from the asthenosphere and subsequently underplated the continental mass, as suggested by Brooks et al. (1976). As a result of this fractionation, the eclogite might have REE contents sufficient to generate the enriched REE contents that are observed in the intermediate magma types of the suite.

Negative Eu anomalies in the REE distributions of the trachyte and rhyolite samples suggest that those magma types may have been significantly altered by low pressure fractional crystallization. If this is true, then the parent magmas from which they evolved were probably similar in composition to the trachyandesite or rhyodacite and were probably generated through partial melting of similar eclogite source materials. Variations among the different primary magmas probably reflects compositional heterogeneity within the eclogite source regime as well as differences in the conditions and extent of the melting process.

The lamprophyre would require a more mafic source, such as garnet peridotite. Since upper-mantle peridotites would be expected to be less enriched in REE than the eclogitic lower lithosphere, the degree of melting required to produce the same REE enrichment in the resulting magma would have to be much lower.

Mechanisms of Magma Generation

Mechanisms responsible for the melting of such materials could include either lithospheric plate subduction or thermal upwelling from the asthenosphere or mesosphere. Lipman et al. (1971) suggested that an imbricate subduction system existed beneath much of the western portion of the North American continent from the beginning of the Laramide orogeny to late Oligocene. Their interpretation was based on the observation that K_2O/SiO_2 ratios of volcanic rocks of that time period generally increase eastward. They utilized the method of Hatherton and Dickinson (1969), which relates the K_2O/SiO_2 ratio to the depth of modern Benioff zones.

Smith (1979) related mafic and intermediate magma at the Spanish Peaks igneous complex to partial melting of mantle and lower crust during the incipient stages of development of the Rio Grande rift. This interpretation could also apply to the Rosita Hills suite. As discussed in the following section, there are many significant similarities in composition between the Rosita Hills and Spanish Peaks provinces. The two provinces lie in close proximity to one another, and both are situated along the northern axis of the Rio Grande structural trend as defined by Seagar and Morgan (1979).

Comparisons to Nearby Igneous Suites of Similar Geologic Age

Two middle Tertiary igneous provinces in close proximity to the Rosita Hills district have been extensively analyzed geochemically. These provinces are the Spanish Peaks hypabyssal

complex and the Summer Coon volcano. The Spanish Peaks complex is located approximately 45 miles to the southeast of the Rosita Hills. It has been dated radiometrically to be 20 to 25 million years old and its chemical properties have been investigated by Knopf (1936), Cullers and Arnold (1980), Jahn (1973), and Jahn et al. (1979). The Summer Coon volcano is situated about 50 miles west-southwest of the Rosita Hills and has been determined to be Oligocene in age. A major and trace element study of the province was conducted by Zielinski and Lipman (1976).

Both the Spanish Peaks complex and the Summer Coon volcano contain rock types that are very similar chemically to rock units within the Rosita Hills district. This is illustrated in Table 10 that compares major element compositions in analagous rock types in the three provinces. Table 11 compares REE contents of corresponding units.

Lamprophyre dikes in the Spanish Peaks are similar to sample RH-49 from the Rosita Hills but some contain significantly more K_2O and much less Na_2O . In terms of REE content, they are identical within the limits of error in the analytical technique.

The rhyolite sample, RH-4, from the Rosita Hills has many similarities to a microgranite sample from the Spanish Peaks and a rhyolite sample from Summer Coon. Each is high in silica and the alkalies, but the Summer Coon rhyolite has much more CaO than the other two samples. REE concentrations are very similar in the Rosita Hills rhyolite and the Spanish Peaks microgranite. The chondrite-normalized plots of the

TABLE 11 Comparison of major element concentrations in Rosita Hills samples with analyses of rocks from nearby igneous suites of similar age

	rhyolite Rosita Hills RH-4	rhyolite Silver Cliff (a)	rhyolite Summer Coon (b)	microgranite Spanish Peaks (c)	rhyodacite Rosita Hills RH-5	rhyodacite Summer Coon (d)
SiO ₂	74.6	75.3	71.2	74.3	64.1	62.7
Al ₂ O ₃	12.1	13.3	14.7	13.7	15.1	15.6
K ₂ O	4.66	7.64	4.45	4.08	3.47	3.05
Na ₂ O	3.87	1.93	4.60	4.94	4.73	4.15
CaO	0.30	0.40	2.05	0.31	3.21	4.33
MgO	0.06	0.13	0.18	0.75	0.38	2.73
Fe ₂ O ₃ *	0.61	0.42	0.85	0.50	3.42	4.63
TiO ₂	0.10	-	0.19	0.03	0.57	0.68
MnO	0.10	tr	0.07	-	0.11	0.10

(a) average of 2 samples; Cross (1896)

(b) average of 2 samples; Zielinski and Lipman (1976)

(c) average of 2 samples; Cullers and Arnold (1980)

(d) average of 3 samples; Zielinski and Lipman (1976)

*representing total Fe content

TABLE 11 Comparison of major element concentrations in Rosita Hills samples
with analyses of rocks from nearby igneous suites of similar age
(Continued)

	lamprophyre Rosita Hills RH-49	lamprophyre Spanish Peaks (a)	syenodiorite Rosita Hills RH-22	syenodiorite Spanish Peaks (b)	latite Rosita Hills RH-43	quartz latite Summer Coon (c)
SiO ₂	45.7	43.3	49.3	54.3	60.5	67.0
Al ₂ O ₃	13.0	11.6	16.5	16.9	15.8	16.6
K ₂ O	1.11	4.02	3.43	2.6	4.34	4.22
Na ₂ O	3.71	1.88	4.44	4.4	4.69	4.30
CaO	10.19	9.82	8.39	5.4	3.41	2.50
MgO	10.79	8.01	3.67	3.0	0.87	0.79
Fe ₂ O ₃ *	10.42	11.28	9.28	7.8	6.12	2.57
TiO ₂	1.34	3.12	1.37	1.3	1.16	0.41
MnO	0.66	-	0.68	-	0.68	0.03

(a) average of 3 samples; Cullers and Arnold (1980)

(b) average of 3 samples; Cullers and Arnold (1980)

(c) Zielinski and Lipman (1976)

*representing total Fe content

TABLE 12 Comparison of REE concentrations in Rosita Hills samples with analyses of rocks from nearby igneous suites of similar age (Continued)

	lamprophyre Rosita Hills RH-49	lamprophyre Spanish Peaks (a)	trachyte Rosita Hills RH-7	syenite Spanish Peaks (a)	rhyolite Rosita Hills RH-4	granite Spanish Peaks (a)
La	69	61	79	63	34	34
Ce	123	129	126	118	51	62
Sm	9.3	10.8	4.5	6.8	2.4	3.1
Eu	2.3	2.7	0.8	1.9	0.2	0.7
Yb	1.6	1.9	2.6	2.4	1.9	1.3
Lu	0.30	0.30	0.50	0.37	0.40	0.19
REE	281	291	279	262	126	136
La/Lu	230	202	158	169	85	177

(a) Cullers and Arnold (1980)

two samples show similar degrees of enrichment and fractionation (La/Lu) and have substantial negative Eu anomalies. The Summer Coon rhyolite has about the same degree of enrichment and fractionation but has only a slight negative Eu anomaly.

A latite sample, RH-43, from the Rosita Hills is similar in some respects to a quartz latite sample from Summer Coon. They have approximately the same alkali content, but the Summer Coon sample has more silica and less CaO and total Fe. REE concentrations differ markedly between the two samples; the Rosita Hills sample has much higher concentrations. The degree of La/Lu fractionation is somewhat greater in the Rosita Hills sample. Neither sample has any substantial Eu anomaly.

Syenodiorite samples from Spanish Peaks are similar to syenodiorite samples from the Rosita Hills. REE concentrations in Rosita Hills sample RH-22 are slightly greater than corresponding Spanish Peaks syenodiorite samples, and the Rosita Hills sample has a slightly greater La/Lu ratio. No Eu anomaly is evident in either of the two rock types.

Conclusions

Geochemical data for the Rosita Hills volcanic province, when coordinated with petrography and field relations, are consistent with the following conclusions concerning the petrogenesis of the rock suite:

(1) While the diversity of the suite is to some extent probably the result of differentiation by fractional crystallization, there is evidence that suggests that the various magma types could not have evolved from a common parent liquid. The trends observed on compositional variation diagrams of the suite at best probably represent the superimposed liquid lines of descent of several similar parent liquids that evolved in a similar manner. Although most major-element variations can be explained in terms of a simple fractional crystallization model, variations in several trace elements (especially Ba and REE) seem to contradict their expected behavior in such a process.

Certain pairs of magma types within the suite, however, bear evidence of a common parent. Major-element data, trace-element data, field relations, and petrography are consistent with a model in which the latite (Tp) magma represents a differentiate of the trachyandesite (Tb). The available data are also consistent with the possibility that the syenodiorite (Tbs) could have evolved from the same liquid from which the lamprophyre (Tl) dikes were derived.

(2) REE distributions of the suite are enriched in light REE (La, Ce) relative to heavy REE (Yb, Lu). This enrichment suggests that the magmas probably originated through partial melting of a garnet-bearing, high pressure mineral assemblage such as eclogite or garnet peridotite. A likely source material for the intermediate to rhyolitic magma types of the Rosita Hills suite is lower-lithospheric eclogite. If such eclogite possessed concentrations of large-ion lithophile elements comparable to concentrations in typical continental basalt, then the eclogite would be capable of generating the fractionated REE distributions of the suite. Initial $^{87}\text{Sr}/^{86}\text{Sr}$ ratios of the intermediate and rhyolitic rock types of the suite range from 0.7057 to 0.7074, which is somewhat higher than would be expected in direct partial melting products of upper-mantle garnet peridotite. The ratios are consistent, however, with partial melting a lower lithospheric eclogite which itself may represent an ancient partial melting derivative of the mantle.

The lamprophyre (Tl) and syenodiorite (Tbs) require a more mafic source material and may be products of partial melting of garnet peridotite. Trace-element concentrations require that either the degree of melting in such a process be small (less than 10 percent) or else that some other process, such as interaction with fluids, greatly altered the REE concentrations in these magma types.

REFERENCES

- Anderson, J.L. and Cullers, R.L., 1978, Geochemistry and evolution of the Wolf River Batholith, a Late Precambrian rapakivi massif in north Wisconsin, U.S.A. *Precambrian Res.*, v. 7, p. 287-324.
- Arnold, B., 1977, Petrogenesis of the Spanish Peaks igneous complex, Colorado: major element, rare earth element, and Sr isotope data. M.S. Thesis, Kansas State Univ., 62 p.
- Arth, J.G. and Hanson G.N., 1975, Geochemistry and origin of early Precambrian crust of northeastern Minnesota. *Geochim. Cosmochim. Acta*, v. 39, p. 325-362.
- Bachinski, S.W. and Scott, R.B., 1979, Rare earth and other trace element contents and the origin of minettes (mica lamprophyres). *Geochim. Cosmochim. Acta*, v. 43, p. 93-100.
- Boettcher, A.L., 1973, Volcanism and orogenic belts - the origin of andesite. *Tectonophysics*, v. 17, p. 231-244.
- Bowen, N.L., 1928, The evolution of igneous rocks. Princeton University Press, 334 p.
- Boyer, R.E., 1962, Petrology and structure of the southern Wet Mountains, Colorado. *Bull. Geol. Soc. Amer.*, v. 73, p. 1047-1070.
- Brooks, C.; James, D.E.; and Hart, S.R., 1976, Ancient lithosphere: its role in young continental volcanism. *Science*, v. 193, p. 1086-1095.
- Carmichael, I.S.E.; 1964, The petrology of Thingmuli, a Tertiary volcano in eastern Iceland. *Jour. Petrol.*, v. 5, p. 435-460.
- Carmichael, I.S.E.; Turner, F.J.; and Verhoogan, J., 1974, Igneous petrology. New York: McGraw Hill, 739 p.
- Chapin, C.E. and Epis, R.C., 1964, Some stratigraphic and structural features of the Thirtynine Mile volcanic field, central Colorado. *Mountain Geologist*, v. 1, no. 3, p. 145-160.
- Chaudhuri, S., 1966, The geochronology of the Keeweenawan rocks of Michigan and the origin of the copper deposits. Ph.D. Dissertation, Ohio State University, 200 p.
- Chaudhuri, S. and Brookins, D.G., 1969, The isotopic age of the Flathead Sandstone, Montana. *Jour. Sed. Pet.*, v. 39, p. 364-368.

- Christiansen, R.L. and Lipman, P.W., 1972, Cenozoic volcanism and plate tectonic evolution of the western United States, II, Late Cenozoic. Royal Soc. London. Phil. Trans., v. 271, p. 249-284.
- Christman, R.A.; Brock, M.R.; Pearson, R.C.; and Singwald, Q.D., 1959, Geology and thorium deposits of the Wet Mountains, Colorado. Progress report: U.S. Geol. Survey Bull. 1072 H, p. 491-535.
- Clark, R.N., 1879, The Humboldt-Pocahontas vein, Rosita, Colorado. Am. Inst. Mining Engineers Trans., v. 7, p. 21-33.
- Cox, K.G.; Bell, J.D.; and Pankhurst, R.J., 1979, The interpretation of igneous rocks. London: Allen and Unwin, 450 p.
- Cross, W., 1896, Geology of Silver Cliff and Rosita, Colorado. U.S. Geol. Survey 17th Annual Report, pt. 2, p. 263-402.
- Cullers, R.L. and Arnold, B., 1980, Geochemistry of the Tertiary Spanish Peaks igneous complex, Colorado, U.S.A. (submitted for publication).
- Cullers, R.L.; Medaris, L.G.; and Haskin, L.A., 1973, Experimental studies of the distribution of rare earths as trace elements among silicate minerals and liquids and water. Geochim. Cosmochim. Acta, v. 37, p. 1499-1512.
- Denechaud, E.B.; Halmke, P.A.; and Haskin, L.A., 1970, Analysis for the rare earth elements by neutron activation and Ge(Li) spectrometry. Jour. Radioanal. Chem., v. 6, p. 97-113.
- Emmons, S.F., 1896, The mines of Custer County, Colorado. U.S. Geol. Survey 17th Annual Report, pt. 2, p. 405-472.
- Faure, G. and Powell, J.L., 1972, Strontium isotope geology. New York, Springer-Verlag, 464 p.
- Flanagan, F.J., 1976, 1972 compilation of data on U.S.G.S. standards. U.S. Geol. Survey Prof. paper 840, p. 131-183.
- Frey, F.A., 1979, Trace element geochemistry: applications to the igneous petrogenesis of terrestrial rocks. Rev. Geophysics and Space Physics, v. 17, no. 4, p. 803-823.
- Frey, F.A.; Haskin, L.A.; and Haskin, M.A., 1971, Rare Earth abundances in some ultramafic rocks. Jour. Geophys. Res., v. 76, p. 2057-2069.
- Frey, F.A.; Haskin, M.A.; Poetz, J.; and Haskin, L.A., 1968, Rare earth abundances in some basic rocks. Jour. Geophys. Res., v. 73, p. 6085-6097.

- Gast, P.W., 1968, Trace element fractionation and the origin of tholeiitic and alkaline magma types. *Geochim. Cosmochim. Acta*, v. 32, p. 1189-1200.
- Gill, J.B., 1974, Role of underthrust oceanic crust in the genesis of a Fijian calc-alkaline suite. *Contr. Mineral. Petrol.*, v. 43, p. 29-45.
- Gordon, G.E.; Randle, K.; Goles, G.; Corliss, J.; Beeson, M.H.; and Osley, S.S., 1968, Instrumental neutron activation analysis of standard rocks with high resolution gamma ray detectors. *Geochim. Cosmochim. Acta*, v. 32, p. 369-396.
- Grabill, L.R., 1883, On the peculiar features of the Bassick mine. *Am. Inst. Mining Engineers Trans.*, v. 11, p. 110-117.
- Green, D.H., 1971, Composition of basaltic magmas as indicators of conditions of origin: application to oceanic volcanism. *Royal Soc. London Phil. Trans.*, v. A268, p. 707-725.
- Green, D.H., 1973, Experimental melting studies on a model upper mantle composition at high pressure under water-saturated and water-unsaturated conditions. *Earth Planet. Sci. Lett.*, v. 19, p. 37-58.
- Green, D.H. and Ringwood, A.E., 1968, Genesis of the calc-alkaline igneous suite. *Contr. Mineral. Petrol.*, v. 18, p. 105-162.
- Haskin, L.A.; Allen, R.O.; Helmke, P.A.; Pastor, T.P.; Anderson, M.R.; Korotev, R.S. and Zweifel, K.A., 1970, Rare earths and other trace elements in Apollo II lunar samples. *Proc. Apollo II Lunar Sci. Conf.*, suppl. 1, v. 2, p. 1213-1231.
- Haskin, L.A.; Haskin, M.A.; Frey, F.A.; and Wildman, T.R., 1968, Relative and absolute terrestrial abundances of the rare earths. In Ahrens, L.H., ed., *Origin and distribution of the elements*. New York: Pergamon, v. 7, p. 929-939.
- Hatherton, T. and Dickinson, W.R., 1969, The relationship between andesitic volcanism and seismicity in Indonesia, the Lesser Antilles, and other island arcs. *Jour. Geophys. Res.*, v. 74, p. 5301-5310.
- Hertogen, J. and Gijbels, R., 1976, Calculation of trace element fractionation during partial melting. *Geochim. Cosmochim. Acta*, v. 40, p. 313-322.
- Higuchi, H. and Nagasawa, H., 1969, Partition of trace elements between rock forming minerals and host volcanic rocks. *Earth Planet. Sci. Lett.*, v. 7, p. 281-287.
- Hill, R. and Boettcher, A.L., 1970, Water in the earth's mantle: melting curves of basalt-water and basalt-water-CO₂. *Science*, v. 167, p. 980-982.

- Hyndman, D.W., 1972, Petrology of igneous and metamorphic rocks. New York: McGraw-Hill, 533 p.
- Ito, K., and Kennedy, G.C., 1967, Melting and phase relations in a natural peridotite to 40 kilobars. *Am. Jour. Sci.*, v. 265, p. 519-538.
- Jacobs, J.W.; Korstev, R.L.; Blanchard, D.P.; and Haskin, L.A., 1977, A well tested procedure for instrumental neutron activation analysis of silicate rocks and minerals. *Jour. Radioanal. Chem.*, v. 40, pp. 93-114.
- Jahn, B., 1973, A petrogenic model for the igneous complex in the Spanish Peaks region, Colorado. *Contr. Mineral. Petrol.*, v. 41, p. 241-258.
- Jahn, B.; Sun, S.S.; and Nesbitt, T., 1979, REE distribution and petrogenesis of the Spanish Peaks igneous complex, Colorado. *Contr. Mineral. Petrol.*, v. 70, p. 281-298.
- Jordan, T.H., 1979, The deep structure of the continents. *Sci. Am.*, v. 240, no. 1, p. 92-107.
- Johnson, R.B., 1968, Geology of the igneous rocks of the Spanish Peaks region, Colorado. U.S. Geol. Survey Prof. Paper 594-G.
- Kay, W.R. and Gast, P.W., 1973, The rare earth content and origin of alkali-rich basalts. *Jour. Geol.*, v. 81, p. 653-682.
- Kilbane, N.A., 1978, Petrogenesis of the McClure Mountain mafic-ultramafic and alkalic complex, Fremont County, Colorado. M.S. Thesis, Kansas State Univ., 158 p.
- Kleinkopf, D.; Peterson, D.L.; and Mattick, R.E., 1979, Gravity, magnetic, and seismic studies of the Silver Cliff and Rosita Hills volcanic area, Colorado. U.S. Geol. Survey Prof. Paper 726-F.
- Knopf, A., 1936, Igneous geology of the Spanish Peaks region, Colorado. *Bull. Geol. Soc. Amer.*, v. 47, p. 1727-1784.
- Koch, R.J., 1978, Petrogenesis of the Precambrian Bevos and Musco groups, St. Francois Mountains igneous complex, Missouri. M.S. Thesis, Kansas State Univ., 102 p.
- Kushiro, I.; Shimizu, N.; Nakamura, Y.; and Akimoto, S., 1972, Composition of coexisting liquid and solid phases formed upon melting of natural garnet and spinel lherzolites at high pressures: a preliminary report. *Earth Planet. Sci. Lett.*, v. 14, p. 19-25.
- Larsen, E.S., 1938, Some new variation diagrams for groups of igneous rocks. *Jour. Geol.*, v. 46, p. 505-520.

- Lipman, P.W.; Doe, B.R.; Hedge, C.E.; and Steven, T.A., 1978, Petrologic evolution of the San Juan volcanic field, southwestern Colorado: Pb and Sr isotopic evidence. *Bull. Geol. Soc. Amer.*, v. 89, pp. 59-82.
- Lipman, P.W.; Protska, H.J.; and Christiansen, R.L., 1971, Evolving subduction zones in the western United States as interpreted from igneous rocks. *Science*, v. 174, p. 821-825.
- Mysen, B. and Boettcher, A.L., 1975, Melting of hydrous mantle: I. Phase relations of natural peridotite at high pressures and temperatures as a function of controlled activities of water, hydrogen, and carbon dioxide. *Jour. Petrol.*, v. 16, p. 520-548.
- Nagasawa, H. and Schnetzler, C.C., 1971, Partitioning of rare earth, alkalic, and alkaline earth elements between phenocrysts and acidic igneous magma. *Geochim. Cosmochim. Acta*, v. 35, p. 953-968.
- Nagasawa, H.; Wakita, H.; Higuchi, H.; and Onuma, N., 1969, Rare earths in peridotite nodules: An explanation of the genetic relationship between basalt and peridotite nodules. *Earth Planet. Sci. Lett.*, v. 5, p. 377-381.
- Nicholls, I.A. and Ringwood, A.E., 1973, Effects of water on olivine stability in tholeiites and the production of silica saturated magmas in island arc environment. *Jour. Geol.*, v. 81, p. 285-300.
- O'Hara, M.J., 1977, Geochemical evolution during fractional crystallization of a periodically refilled magma chamber. *Nature*, v. 266, p. 503-507.
- Onuma, N.; Higuchi, H.; Wakita, H.; Nagasawa, H., 1968, Trace element partition between two pyroxenes and the host volcanic rocks. *Earth Planet. Sci. Lett.*, v. 5, p. 47-51.
- Oxburgh, E.R. and Turcotte, D.L., 1970, The thermal structure of island arcs. *Bull. Geol. Soc. Amer.*, v. 81, p. 1665-1688.
- Pankhurst, R.J., 1977, Open system crystal fractionation and variation in incompatible elements in basalts. *Nature*, v. 268, p. 36-38.
- Peacock, M.A., 1931, Classification of igneous rocks. *Jour. Geol.*, vol. 39, p. 54-67.
- Philpotts, J.A. and Schnetzler, C.C., 1968, Europium anomalies and the genesis of basalt. *Chem. Geol.*, v. 3, p. 5-13.

- Reid, J.B. and Frey, F.A., 1971, Rare earth distributions in lherzolite and garnet pyroxenite xenoliths and the constitution of the upper mantle. *Jour. Geophys. Res.*, v. 76, p. 1184-1196.
- Reitz, B., 1980, Evolution of Tertiary plutonic and volcanic rocks near Revenna, Granite County, Montana. M.S. Thesis. Kansas State Univ., 92 p.
- Ringwood, A.E., 1969, Composition and evolution of the upper mantle. *Amer. Geophysical Union Monograph* 13, p. 1-17.
- Ringwood, A.E., 1974, The petrological evolution of the island arc systems. *Jour. Geol. Soc., London*, v. 130, p. 183-204.
- Rock, N.M.S., 1977, The nature and origin of lamprophyres: some definitions, distinctions, and derivations. *Earth Sci. Rev.*, v. 13, p. 123-169.
- Roden, M., 1977, Rare earth element distributions and strontium isotope data from the Gem Park igneous complex, Colorado. M.S. Thesis, Kansas State Univ., 103 p.
- Schnetzler, C.C. and Philpotts, J.A., 1968, Partition coefficients of rare earth elements and barium between igneous matrix material and rock-forming mineral phenocrysts. In Ahrens, L.H., ed., *Origin and distribution of the elements*. New York: Pergamon. v.7, p. 929-939.
- Schnetzler, C.C. and Philpotts, J.A., 1970, Partition coefficients of some rare earth elements between igneous matrix material and rock-forming mineral phenocrysts. *Geochim. Cosmochim. Acta*, v. 34, p. 331-340.
- Scott, G.R. and Taylor, R.B., 1975, Post-Paleocene Tertiary rocks and Quaternary volcanic ash of the Wet Mountain Valley, Colorado. *U.S. Geol. Survey Prof. Paper* 868, 15 p.
- Seager, W.R., and Morgan, P., 1979, Rio Grande rift in southern New Mexico, West Texas, and northern Chihuahua. In Riecker, R.E., ed., *Rio Grande rift: tectonics and magmatism*. *Amer. Geophysical Union special publication*. 438 p.
- Sharp, W.N., 1978, Geologic map of the Silver Cliff and Rosita Hills volcanic centers, Custer County, Colorado. *U.S. Geol. Survey map* I-1081.
- Shaw, D.M., 1970, Trace element fractionation during anatexis. *Geochim. Cosmochim. Acta*, v. 34, p. 237-243.
- Shibata, T.; Thompson, G.; and Frey, F., 1979, Tholeiitic and alkali basalts from the Mid-Atlantic ridge at 43°N. *Contr. Mineral. Petrol.*, v. 70, p. 127-141.

- Siems, P.L., 1967, Volcanic and economic geology of the Rosita Hills and Silver Cliff districts, Custer County, Colorado. Ph.D. Dissertation, Colo. School Mines, 222 p.
- Siems, P.L., 1968, Volcanic geology of the Rosita Hills and Silver Cliff district, Custer County Colorado. Colo. School Mines Quarterly, v. 63, p. 89-124.
- Smalley, J., and Cullers, R., 1980, Geochemistry of the Rosita Hills and Silver Cliff volcanic centers of southern Colorado. Geol. Soc. Amer. Abstracts, v. 12, p. 16.
- Smith, R.P., 1979, Early rift magmatism at Spanish Peaks, Colorado. In Riecker, R.E., ed., Rio Grand rift: tectonics and magmatism. Amer. Geophysical Union special publication. 438 p.
- Spaid-Reitz, M., 1980, Petrogenesis of a bi-modal assemblage of alkali-basalt and rhyolitic ignimbrite, Gravelly Range, southwest Montana. M.S. Thesis, Kansas State Univ., 94 p.
- Streckeisen, A., 1976, To each plutonic rock its proper name. Earth Sci. Rev., v. 12, p. 1-33.
- Suhr, N.H. and Ingamells, 1966, Solution technique for analysis of silicates. Analytical Chem., v. 38, no. 6, p. 730-734.
- Thornton, C.P. and Tuttle, O.F., 1960, Chemistry of igneous rocks: I. differentiation index. Am. Jour. Sci., v. 258, p. 664-684.
- Tweto, O., 1979, The Rio Grande rift system in Colorado. In Riecker, R.E., ed., Rio Grande rift: tectonics and magmatism. Amer. Geophysical Union special publication. 438 p.
- Wulsten, C., 1876, The silver region of the Sierra Mojada (Wet Mountains) and Rosita, Fremont County, Colorado. Rosita: Bank of Rosita.
- Yoder, H.S. and Tilley, C.E., 1962, Origin of basalt magmas: an experimental study of natural and synthetic rock systems. Jour. Petrol., v. 3, p. 342-532.
- Zielinski, R.A. and Lipman, P.W., 1976, Trace element variations at Summer Coon volcano, San Juan Mountains, Colorado, and the origin of continental-interior andesite. Bull. Geol. Soc. Amer., v. 87, p. 1477-1485.

APPENDIX I: Petrographic descriptions

Appendix I contains petrographic descriptions of rock samples analyzed chemically in this study. Modal percentages listed with each description are based on visual estimations. Anorthite contents in plagioclase phenocrysts were estimated using the Michel-Levy method. Schematic drawings of the thin sections are intended to illustrate the textural character of each rock specimen as well as indicate the relative sizes and inter-relationships of the various mineral phases.

Sample Number: RH-49

Classification: OLIVINE VOGESITE
(LAMPROPHYRE)

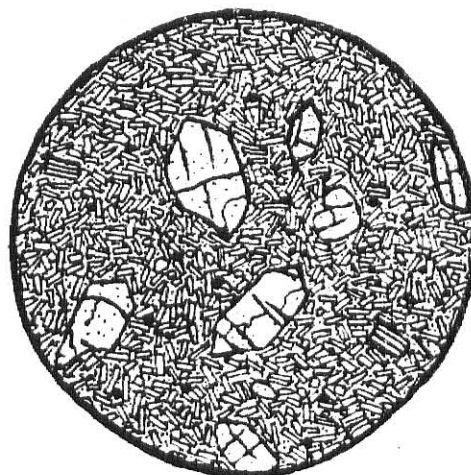
Sampling location: Small dike in Wilmer gulch about 2 miles
south of Rosita
(NW $\frac{1}{4}$; NE $\frac{1}{4}$; NW $\frac{1}{4}$; Sec. 9; T23S, R71W)

Texture: Microporphyritic, panidiomorphic

Olivine occurs as euhedral to subhedral phenocrysts which are generally less than 1.0 mm in diameter. Plagioclase (An 30) occurs as phenocrysts and as the major constituent of the groundmass. Clinopyroxene is present as euhedral crystals less than 0.2 mm in diameter. The groundmass matrix is glass.

Modal Distribution:

Olivine.....	20%
Plagioclase.....	55%
Clinopyroxene.....	5%
Black oxides.....	5%
Glass.....	15%



0 0.5 1.0 1.5 2.0
mm

Sample Number: RH-22

Classification: SYENODIORITE

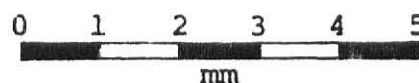
Sampling Location: Southeast slope of Mt. Fairview in Goodhope
Gulch approximately 2 miles northwest of
Rosita (SW $\frac{1}{4}$; SW $\frac{1}{4}$; SE $\frac{1}{4}$; Sec. 19; T22S; R71W)

Texture: Hypidiomorphic-granular

Plagioclase (An 25-30) occurs as euhedral to subhedral crystals ranging in size from less than 0.1 mm to greater than 3 mm in length. Larger plagioclase crystals tend to exhibit complex oscillatory zoning. Augite crystals are pale green and are generally larger than the plagioclase ranging up to 3 mm long. Orthoclase crystals range from 0.1 mm to 0.8 mm in length. Biotite crystals are interstitial in nature and are generally less than 0.5 mm in diameter. Minor anhedral nepheline occurs as an interstitial component.

Modal Distribution:

Plagioclase.....	45%
Orthoclase.....	15%
Augite.....	30%
Biotite.....	5%
Black oxides.....	5%
Nepheline.....	Tr



Sample Number: RH-23

Classification: PYROXENE ANDESITE

Sampling Location: Top of Paris Hill about 2 miles northwest of Rosita (NW $\frac{1}{4}$; NE $\frac{1}{4}$; NW $\frac{1}{4}$; Sec. 30; T22S; R71W)

Texture: Porphyritic with cryptofelsic groundmass

Plagioclase (An 20-25) occurs as large euhedral single crystals up to 4 mm in length and in combination with augite and magnetite in glomeroporphyritic clusters. Single augite crystals commonly contain inclusions of magnetite and tend to be euhedral ranging up to 3 mm in long dimension. Sanidine-anorthoclase occurs as small euhedral crystals less than 1.0 mm in length. Magnetite also occurs as subhedral to euhedral crystals up to 0.3 mm in diameter within the groundmass.

Modal Distribution:

Plagioclase.....	30%
Sanidine-anorthoclase.....	5%
Clinopyroxene.....	20%
Black oxides.....	5%
Cryptofelsic groundmass....	40%



Sample Number: RH-39

Classification: TRACHYANDESITE

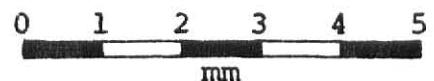
Sampling Location: Top of Bunker Hill 2 miles northwest of Rosita
(NE $\frac{1}{4}$; SW $\frac{1}{4}$; SW $\frac{1}{4}$; Sec. 17; T22S; R71W)

Texture: Fine grained porphyritic with cryptofelsic groundmass

Subhedral to euhedral plagioclase (An₂₀) occurs as the predominant phenocryst ranging from less than 1.0 mm to greater than 4.0 mm in length. Some of the larger plagioclase crystals are slightly zoned. Sanidine-anorthoclase is somewhat less abundant and occurs primarily as smaller euhedral crystals in the range of 0.5 mm to 1.5 mm in length. Elongate green hornblende phenocrysts range up to 3.5 mm in length and occur occasionally in clusters. Euhedral augite and biotite occur in minor amounts and are less than 1.0 mm in diameter. Apatite occurs as inclusions in the hornblende.

Modal Distribution:

Plagioclase.....	25%
Sanidine-anorthoclase.....	15%
Hornblende.....	5%
Biotite.....	3%
Augite.....	2%
Black oxides.....	5%
Apatite.....	Tr
Cryptofelsic groundmass....	45%



Sample Number: RH-27

Classification: TRACHYANDESITE

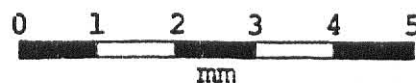
Sampling Location: Northern end of Goodhope Gulch east of
Lookout Mt. (SW $\frac{1}{4}$; SW $\frac{1}{4}$; NE $\frac{1}{4}$; Sec. 19; T22S;
R71W)

Texture: Porphyritic with a cryptofelsic groundmass

The predominant phenocrysts are plagioclase, potassium feldspar and green hornblende. Plagioclase (An₂₀) crystals are largely euhedral and range in size from less than 0.5 mm to greater than 4.0 mm in length. Sanidine-anorthoclase occurs as euhedral crystals ranging from less than 0.4 mm in length up to 30. mm in length. Hornblende crystals are elongated and euhedral and occasionally occur in clusters. Clinopyroxene and biotite are present in small amounts. Apatite occurs as inclusions in the hornblende.

Modal Distribution:

Plagioclase.....	15%
Sanidine-anorthoclase.....	10%
Hornblende.....	5%
Biotite.....	2%
Clinopyroxene.....	1%
Apatite.....	Tr
Black oxides.....	5%
Cryptofelsic groundmass....	62%



Sample Number: RH-5

Classification: RHYODACITE

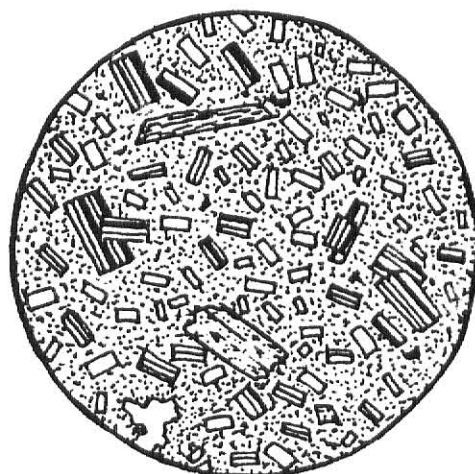
Sampling Location: Southeast slope of Wakefield Hill
(SW $\frac{1}{4}$; NW $\frac{1}{4}$; SW $\frac{1}{4}$; Sec. 33; T22S; R71W)

Texture: Microporphyritic with cryptofelsic groundmass

Euhedral plagioclase (An₂₂) crystals constitute the majority of the phenocrysts and range in size from less than 0.1 mm to about 1.0 mm in length. Sanidine-anorthoclase occurs as smaller euhedral crystals generally less than 0.5 mm in length. Elongate green hornblende phenocrysts range from 0.2 mm to 1.5 mm in length and are altered by weathering. Biotite crystals are pleochroic from yellow to brown and range in size from 0.1 mm to 0.3 mm in diameter. Anhedral quartz occurs as interstitial material in the groundmass.

Modal Distribution:

Plagioclase.....	45%
Sanidine-anorthoclase.....	20%
Hornblende.....	10%
Quartz.....	5%
Biotite.....	2%
Magnetite.....	3%
Cryptofelsic groundmass....	15%



Sample Number: RH-43

Classification: LATITE

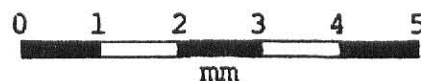
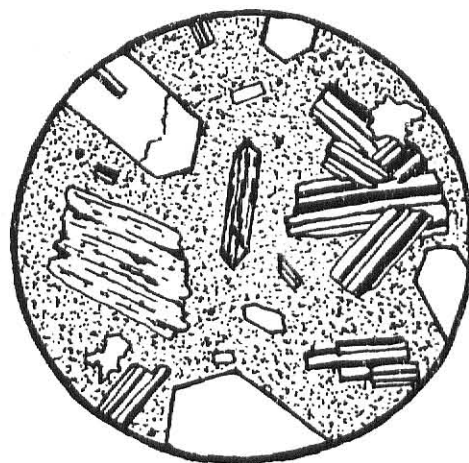
Sampling Location: Small ridge southeast of Pringle Hill
(NW $\frac{1}{4}$; SE $\frac{1}{4}$; NW $\frac{1}{4}$; Sec. 32; T22S; R71W)

Texture: Porphyritic with cryptofelsic groundmass

Sanidine-anorthoclase is present as large euhedral phenocrysts up to 3 mm in length. Euhedral plagioclase (An 18) phenocrysts tend to be slightly smaller than the potassium feldspars and generally occur in clusters. Elongate euhedral green hornblende crystals are generally altered and range from 0.2 to 0.8 mm in length. Quartz is present as an interstitial component of the groundmass. Biotite crystals are pleochroic from yellow to brown and range up to 2 mm in diameter.

Modal Distribution:

Sanidine-anorthoclase.....	25%
Plagioclase.....	15%
Biotite.....	5%
Hornblende.....	5%
Quartz.....	3%
Black oxides.....	2%
Cryptofelsic groundmass....	45%



Sample Number: RH-47

Classification: LATITE

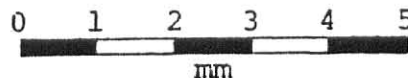
Sampling Location: Small ridge south of Democrat Hill
approximately 1½ miles west of Rosita
(NW¼; SE¼ SE¼; Sec. 30; T22S; R71W)

Texture: Porphyritic with cryptofelsic groundmass

Plagioclase (An 12) phenocrysts range from 0.1 mm to 3.0 mm in length and occasionally occur in clusters. Sanidine-anorthoclase phenocrysts range from 0.1 mm to 3.5 mm in length. Biotite crystals are pleochroic from yellow to brown and range up to 1.5 mm in diameter. Hornblende phenocrysts range up to 1.5 mm in length and are generally altered to oxides. Quartz is interstitial in the groundmass.

Modal Distribution:

Sanidine-anorthoclase.....	20%
Plagioclase.....	15%
Hornblende.....	5%
Biotite.....	3%
Quartz.....	2%
Cryptofelsic groundmass....	55%



Sample Number: RH-8

Classification: TRACHYTE

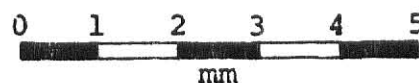
Sampling Location: Top of Pocahontas Hill about $\frac{1}{2}$ mile north of Rosita (NW $\frac{1}{4}$; NE $\frac{1}{4}$; SW $\frac{1}{4}$ Sec. 28; T22S; R71W)

Texture: Porphyritic with pilotaxitic orthophyric groundmass

Sanidine-anorthoclase occurs as large euhedral phenocrysts up to 6 mm in maximum dimension and as the primary constituent of the groundmass. Sodic plagioclase (An 15-18) is present as single crystals up to 1.5 mm in length and as radiating clusters. Most of the larger plagioclase crystals are mantled with sanidine-anorthoclase and plagioclase inclusions occur within the large phenocrysts of sanidine-anorthoclase. Biotite, pleochroic from yellow to brown, ranges from 0.5 mm to 1.0 mm in diameter. Some minor interstitial quartz is present in the groundmass.

Modal Distribution:

Sanidine anorthoclase.....	20%
Plagioclase.....	5%
Biotite.....	3%
Quartz.....	1%
Black oxides.....	1%
Orthophyric groundmass.....	70%



Sample Number: RH-42

Classification: TRACHYTE

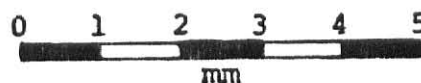
Sampling Location: Approximately $\frac{1}{4}$ mile south of Querida
(SE $\frac{1}{4}$; SE $\frac{1}{4}$; NW $\frac{1}{4}$; Sec. 21; T22S; R71W)

Texture: Porphyritic with pilotaxitic orthophyric groundmass

Sanidine-anorthoclase phenocrysts are generally euhedral and are of varying sizes ranging up to 5 mm in long dimension. The sanidine-anorthoclase occurs in single crystal and twinned forms as well as in glomeroporphyritic clusters with sodic plagioclase (An 16-20) and hornblende. Plagioclase also occurs as solitary phenocrysts ranging up to 2 mm in length. The groundmass contains abundant felsic laths which are presumably plagioclase and K-feldspar. Biotite is present in trace amounts.

Modal Distribution

Sanidine-anorthoclase.....	25%
Plagioclase.....	15%
Hornblende.....	2%
Biotite.....	1%
Black oxides.....	1%
Orthophyric groundmass.....	56%



Sample Number: RH-7

Classification: TRACHYTE

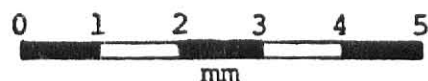
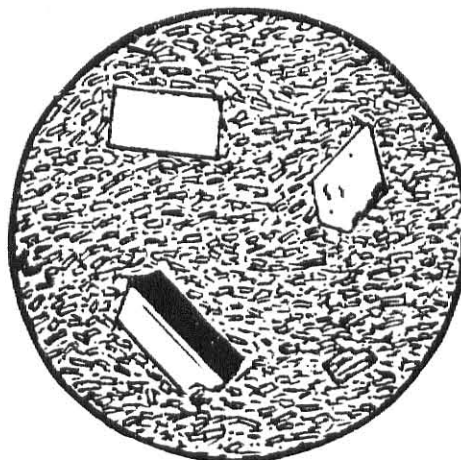
Sampling Location: Dike on top of Pringle Hill
(NW $\frac{1}{4}$; NW $\frac{1}{4}$; SE $\frac{1}{4}$; Sec. 29; T22S; R71W)

Texture: Porphyritic with pilotaxitic orthophyric groundmass

Sanidine-anorthoclase occurs primarily as single crystals up to 4 mm in long dimension. Sodic plagioclase crystals (An 15-19) are euhedral and range up to 2 mm in long dimension. Biotite occurs in small amounts as subhedral phenocrysts which are generally less than 1 mm in long dimension. Black oxides are present and appear to be weathering products of biotite.

Modal Distribution:

Sanidine-anorthoclase.....	25%
Plagioclase.....	5%
Biotite.....	2%
Black oxides.....	1%
Orthophyric groundmass.....	67%



Sample Number: RH-4

Classification: RHYOLITE

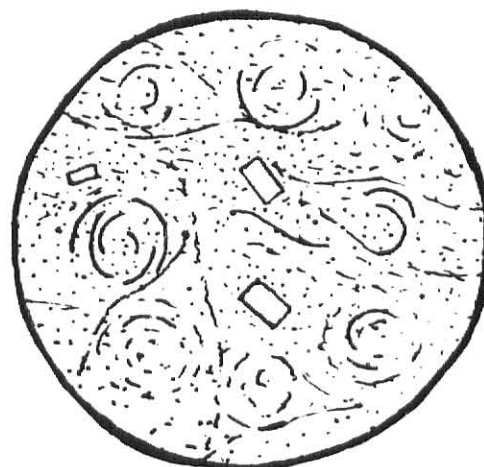
Sampling Location: Small ridge south of Schoolfield Road
(SE $\frac{1}{4}$; NW $\frac{1}{4}$; NW $\frac{1}{4}$; Sec. 6; T23S; R71W)

Texture: Flow-banded glass, slightly porphyritic

The sample consists primarily of flow-banded glass with perlitic cracks. The glassy matrix contains abundant tiny crystallites and a few small phenocrysts of sanidine which are less than 1 mm in length.

Modal Distribution:

Sanidine..... 3%
Glass..... 97%



APPENDIX II: Geochemical data

Appendix II is a compilation of the results of geochemical analyses of volcanic rock samples from the Rosita Hills district. Table 12 lists major element assays of 12 samples with corresponding C.I.P.W. normative compositions. The method of analysis was atomic absorption spectrophotometry. Table 13 lists major element assays provided by Cross (1896). The method of analysis was not discussed in that report. Table 14 lists concentrations of Sc, Co, Ba, Hf, Th, and several rare earth elements including La, Ce, Sm, Eu, Tb, Yb, and Lu. The method of analysis was instrumental neutron activation. Table 15 lists Rb and Sr concentrations in samples as determined by x-ray fluorescence. Sampling locations of samples analyzed in this study are shown on the geologic map in Figure 2 (page 11).

TABLE 13 Major-element analyses (weight-percent oxides) and C.I.P.W. normative compositions of samples examined in this study

	RH-49 LAMPRO- PHYRE (T1)	RH-22 SYENO- DIORITE (Tbs)	RH-23 SYENO- DIORITE (Tbs)	RH-39 TRACHY- ANDESITE (Tb)	RH-27 TRACHY- ANDESITE (Tb)	RH-43 LATITE (Tp)
SiO ₂	45.69	49.37	54.67	56.68	60.75	60.54
Al ₂ O ₃	13.02	16.55	18.60	16.85	18.10	15.85
K ₂ O	1.11	3.43	4.14	3.65	4.09	4.34
Na ₂ O	3.71	4.44	5.23	4.70	5.84	4.69
CaO	10.19	8.39	6.10	4.71	3.90	3.41
MgO	10.79	3.67	2.65	2.38	1.56	0.87
Fe ₂ O ₃ *	10.42	9.28	7.15	5.49	6.12	3.20
TiO ₂	1.34	1.37	1.10	0.93	1.16	0.47
MnO	0.66	0.68	0.56	0.46	0.68	0.45
H ₂ O ⁺	2.31	1.13	1.37	2.08	1.42	3.06
H ₂ O ⁻	0.40	0.26	0.45	0.33	0.38	0.16
Total	99.64	98.57	102.11	98.26	98.67	97.04
Q	-	-	-	-	-	7.53
Or	6.55	20.25	24.44	21.54	24.14	25.62
Ab	10.80	15.19	27.88	29.74	49.37	39.65
An	15.58	15.09	15.04	11.36	11.09	9.37
Ne	11.16	12.11	8.85	-	-	-
Di	28.28	22.14	12.80	10.02	7.02	6.39
Hy	-	-	-	9.05	1.65	3.60
Mt	1.92	1.70	1.31	1.12	1.00	0.58
Il	2.54	2.61	-	1.77	-	-
Ol	19.66	7.73	8.57	-	5.89	-

*representing total Fe content

TABLE 13 Major-element analyses (weight-percent oxides) and C.I.P.W. normative compositions of samples examined in this study (Continued)

	RH-47 LATITE (Tp)	RH-5 RHYODA- CITE (Tbm)	RH-42 TRACHYTE (Tt)	RH-7 TRACHYTE (Tt)	RH-8 TRACHYTE (Tt)	RH-4 RHYO- LITE (Trr)
SiO ₂	62.16	64.12	63.50	64.64	65.50	74.65
Al ₂ O ₃	15.85	15.18	16.65	16.65	16.67	12.10
K ₂ O	4.25	3.47	6.81	5.79	6.03	4.66
Na ₂ O	5.11	4.73	5.24	5.43	5.47	3.87
CaO	3.45	3.21	0.20	0.82	0.83	0.30
MgO	0.79	0.38	0.17	0.18	0.188	0.06
Fe ₂ O ₃ *	4.15	3.42	1.45	1.71	1.92	0.61
TiO ₂	0.59	0.57	0.36	0.48	0.48	0.10
MnO	0.28	0.11	0.05	0.72	0.73	0.10
H ₂ O ⁺	0.31	1.44	1.42	0.97	0.96	1.21
H ₂ O ⁻	0.31	0.49	0.35	0.18	0.21	0.40
Total	97.36	96.82	96.15	97.52	98.91	98.06
Q	6.98	15.38	5.48	7.44	7.20	33.11
Or	25.09	20.48	40.20	34.18	35.59	27.51
Ab	43.20	39.99	44.30	45.90	46.25	32.17
An	7.75	9.93	0.99	3.96	3.12	1.48
Ne	-	-	-	-	-	-
Di	8.46	5.177	-	0.10	0.87	-
Hy	3.17	2.17	2.16	3.60	3.52	-
Mt	0.76	0.60	-	-	-	-
Il	-	0.08	0.68	0.91	0.91	-
Ol	-	-	-	-	-	-

*representing total Fe content

TABLE 14 Major-element analyses of Rosita Hills samples provided by Cross (1896)

	TRACHY- ANDESITE		RHYODACITE		LATITE		TRACHYTE		RHYOLITE	
	(Tb)	(Tbm)	(Tp)	(Tp)	(Tt)	(Tt)	(Ttr)	(Ttr)	(Ttr)	(Ttr)
SiO ₂	57.01	66.46	58.94	63.49	65.41	66.13	70.87	71.20		
Al ₂ O ₃	18.41	17.91	17.19	18.40	18.78	13.10	15.18	13.70		
K ₂ O	3.72	3.74	3.90	4.62	5.41	5.86	5.04	4.90		
Na ₂ O	4.95	4.79	4.20	5.70	5.91	5.22	3.47	2.90		
CaO	4.29	2.89	4.45	2.80	1.58	0.96	1.58	0.50		
MgO	2.34	0.49	1.52	0.66	0.16	0.39	0.60	0.20		
FeO	2.36	0.35	1.98	1.09	0.72	0.22	0.12	-		
Fe ₂ O ₃	3.69	2.42	2.63	2.44	0.94	2.18	2.18	0.90		
TiO ₂	0.27	-	0.27	tr	-	-	tr	0.10		
MnO	0.21	tr	0.10	0.16	tr	tr	tr	-		
P ₂ O ₅	0.42	-	0.23	tr	tr	0.04	tr	-		
H ₂ O	2.29	1.01	4.53	1.04	1.38	0.85	1.08	4.90		

TABLE 15 Concentrations of trace-elements (ppm) in Rosita Hills samples as determined by neutron-activation analysis

	RH-49 LAMPRO- PHYRE	RH-22 SYENO- DIORITE	RH-39 TRACHY- ANDESITE	RH-27 TRACHY- ANDESITE	RH-5 RHYO- DACITE
	(Tl)	(Tbs)	(Tb)	(Tb)	(Tbm)
La	69.4	73.0	69.5	90.1	39.4
Ce	123.6	180.2	111.4	144.9	60.9
Sm	9.3	11.4	7.8	10.6	4.7
Eu	2.3	2.6	2.0	2.4	1.3
Tb	0.7	1.2	0.9	1.0	0.7
Yb	1.6	2.8	2.5	3.3	1.3
Lu	0.3	0.3	0.4	0.4	0.2
Sc	25.5	9.5	8.7	6.3	6.9
Co	47.9	17.5	16.9	18.4	15.7
Ba	1170	1260	1350	1580	730
Hf	3.6	3.9	3.7	5.1	3.7
Th	7.2	11.0	11.9	11.7	7.3
La/Lu*	30	20	21	20	24
REE	281	360	264	342	147

*chondrite normalized values

TABLE 15 Concentrations of trace-elements (ppm) in Rosita Hills samples as determined by neutron-activation analysis (Continued)

	RH-43 LATITE (Tp)	RH-47 LATITE (Tp)	RH-7 TRACHYTE (Tt)	RH-42 TRACHYTE (Tt)	RH-4 RHYOLITE (Trr)
La	75.3	77.8	79.0	82.7	34.4
Ce	120.4	123.9	126.5	125.4	51.1
Sm	6.4	7.5	4.5	5.2	2.4
Eu	1.5	1.7	0.8	0.9	0.2
Tb	0.9	0.9	1.2	1.2	0.9
Yb	2.2	2.6	2.6	2.4	1.9
Lu	0.34	0.39	0.50	0.48	0.4
Sc	3.6	5.5	1.2	1.0	3.1
Co	10.1	9.1	13.5	12.2	13.5
Ba	1430	1670	430	700	130
Hf	6.4	7.4	8.6	10.3	4.5
Th	17.7	16.7	29.8	32.2	32.1
La/Lu*	20	19	20	18	8
REE	273	287	279	284	126
*chondrite normalized values					

Table 16 Strontium and rubidium concentrations (ppm) of Rosita Hills samples as determined by x-ray fluorescence

Lithologic Unit	Sample Number	Rock Name	Rb	Sr	Rb/Sr
Trr	RH-4	Rhyolite	183	40	4.58
Tt	RH-7	Trachyte	178	153	1.16
Tt	RH-42	Trachyte	179	148	1.21
Tt	RH-8	Trachyte	147	439	.33
Tp	RH-43	Latite	107	740	.14
Tp	RH-47	Latite	113	709	.16
Tbm	RH-5	Rhyodacite	53	1098	.05
Tb	RH-27	Trachyandesite	91	1029	.09
Tb	RH-39	Trachyandesite	84	965	.09
Tbs	RH-23	Pyroxene andesite	115	1297	.09
Tbs	RH-22	Syenodiorite	84	1353	.06
Tl	RH-49	Lamprophyre	31	1394	.02

APPENDIX III: Trace-element modeling equations and partition coefficients

Trace element concentrations of hypothetical melts discussed in this report were calculated using the aggregate, non-modal melting equation of Shaw (1970):

$$\frac{C_1}{C_s} = \frac{1}{F} \left[1 - \left(1 - \frac{PF}{D_o} \right)^{1/P} \right]$$

where:

C_1 = trace-element concentration in the derived liquid

C_s = trace-element concentration in the source rock

F = fraction melted

P = proportionality constant

D_o = bulk distribution coefficients

The proportionality constant (P) accounts for the proportions of each phase contributing to the melt as well as the partition coefficient for each phase. It is expressed as:

$$P = P_1K_1 + P_2K_2 + P_3K_3 + \dots$$

where:

P_1 = proportion of phase #1 in the melt

K_1 = partition coefficient of a particular trace element for phase #1

The bulk distribution coefficient (D_o) represents the overall effect of fractionation of a particular element in the anatexis of a multiple phase source rock. It is expressed as follows:

$$D_o = X_1K_1 + X_2K_2 + X_3K_3 + . . .$$

where:

X_1 = fraction of phase #1 in the source

K_1 = the partition coefficient of a particular trace element for phase #1

Changes in trace element concentrations in the melts during fractional crystallization were predicted using the equation of Haskin et al. (1970):

$$\frac{C_1}{C_a} = (1 - X)^K - 1$$

where:

C_1 = concentration of a particular trace element in a residual magma after crystallization and extraction of a particular mineral phase

C_a = concentration of the trace element in the parent magma prior to crystallization of the mineral phase

X = fraction of the parent magma which is crystallized and subsequently extracted

K = partition coefficient

Trace-element partition coefficients used in these modeling equations are listed in Tables 18 and 19 and are graphed in Figures 16 and 17.

TABLE 17: Partition coefficients used in trace-element modeling of basaltic magma.

Mineral:	Olivine	Clino- pyroxene	Horn- blende	Phlogo- pite	Plagio- clase	Garnet	Spinel
Element							
Ce	0.007	0.15	0.20	0.034	0.12	0.028	0.08
Nd	0.0066	0.31	0.33	0.032	0.081	0.068	-
Sm	0.0066	0.50	0.52	0.031	0.067	0.29	0.05
Eu	0.0068	0.51	0.59	0.030	0.34	0.49	0.03
Gd	0.0077	0.61	0.63	0.030	0.063	0.97	-
DY	0.0096	0.68	0.68	0.030	0.055	3.17	-
Yb	0.014	0.62	0.49	0.042	0.067	11.5	0.02
Lu	0.016	0.56	0.43	0.046	0.060	11.9	0.02
K	0.0068	0.038	0.96	2.65	0.17	0.015	-
Rb	0.0098	0.031	0.29	3.06	0.071	0.042	-
Sr	0.014	0.12	0.46	0.081	1.83	0.012	-
Ba	0.001	0.001	0.42	-	0.023	0.002	0.01
Co	3	0.02	4	-	0.02	0.3	10
Cr	2	0.10	2	-	0.10	2	10
Sc	0.003	0.035	10	-	0.035	10	10

Compiled by Arth and Hanson (1975)

Original References: Higuchi and Nagasawa (1969); Nagasawa and Schnetzler (1971);
Onuma et al. (1968); Schnetzler and Philpotts (1968); and
Schnetzler and Philpotts (1970)

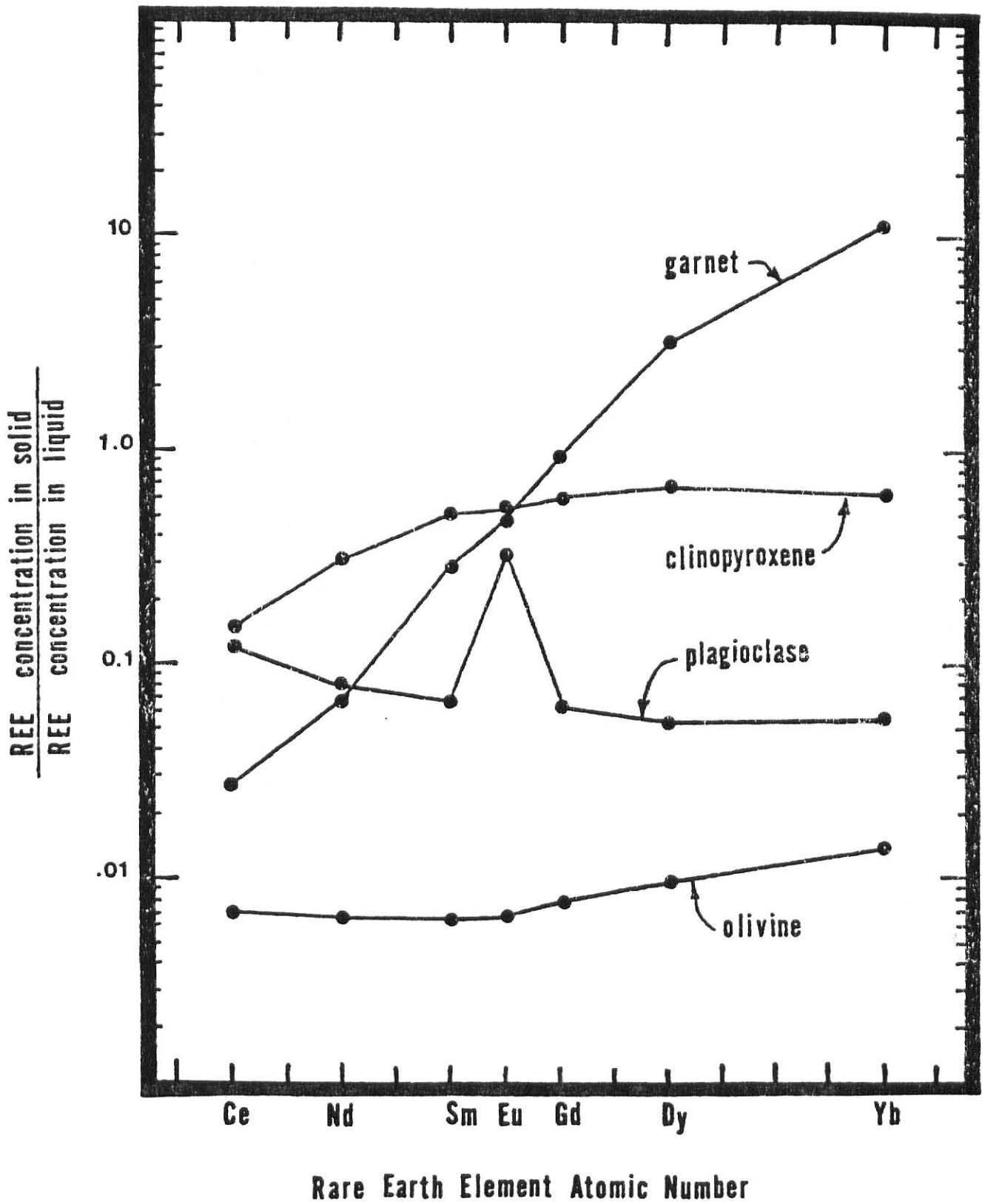


FIGURE 16: Partition coefficients used in trace-element modeling of basaltic magma

TABLE 18: Partition coefficients used in trace-element modeling of silica-rich magma.

Mineral:	Clino- pyroxene	Horn- blende	K- Feldspar	Biotite	Apatite	Plagioclase
Element						
Ce	0.50	1.52	0.044	0.32	34.7	0.27
Nd	1.11	4.26	0.025	0.29	57.1	0.21
Sm	1.67	7.77	0.018	0.26	62.8	0.13
Eu	1.56	5.14	1.13	0.24	30.4	2.15
Gd	1.85	10.0	0.011	0.28	56.3	0.097
Dy	1.93	13.0	0.006	0.29	50.7	0.064
Er	1.66	12.0	0.006	0.35	37.2	0.055
Yb	1.58	8.38	0.012	0.44	23.9	0.049
Lu	1.54	5.5	0.006	0.33	20.2	0.046
K	0.037	0.081	-	-	-	0.10
Rb	0.032	0.014	0.366	2.24	-	0.041
Sr	0.516	0.022	3.87	-	-	4.4
Ba	0.131	0.044	6.12	9.7	-	0.308
Co	5	10	-	20	-	0.10
Cr	12	2	-	12	-	0.06
Sc	10	15	-	11	-	0.02

Compiled by Arth and Hanson (1975)

Original References: Higuchi and Nagasawa (1969); Nagasawa and Schnetzler (1971);
Onuma et al. (1968); Schnetzler and Philpotts (1968); and
Schnetzler and Philpotts (1970)

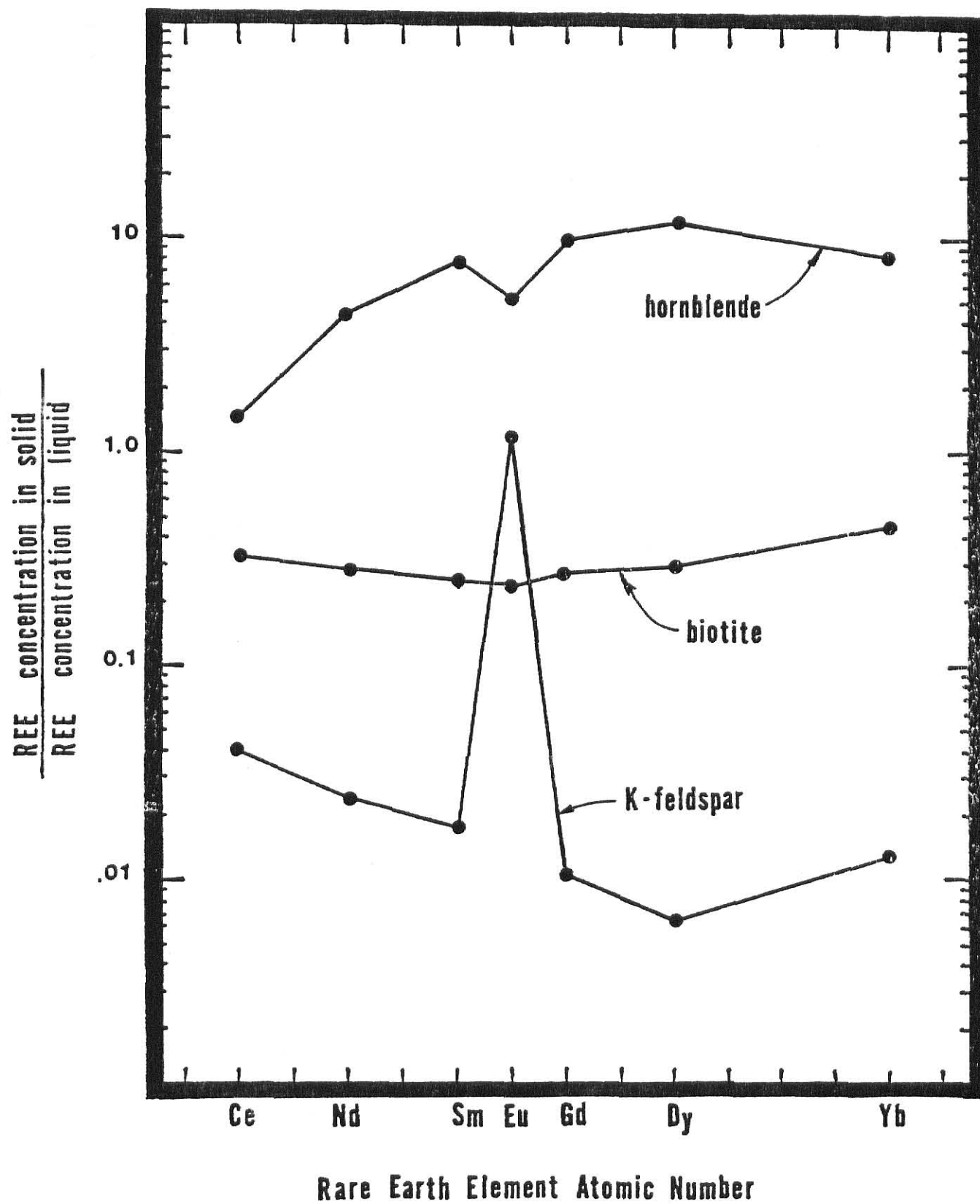


FIGURE 17: Partition coefficients used in trace-element modeling of silica-rich magma

ACKNOWLEDGMENTS

I wish to thank my major professor, Dr. Robert Cullers, for his guidance in this project. I also wish to thank Dr. Henry Beck, Dr. Dean Eckhoff, Dr. Claude Shenkel, and Dr. James Underwood for serving on my thesis advisory committee and for providing constructive editorial suggestions which improved the text.

Several people assisted me in the laboratory during certain parts of the analytical work and their help was very much appreciated. These people included Bruce Reitz, Malia Spaid-Reitz, Richard Robinson, Subramanian Ramakrishnan, Dr. Gerard James, Mark Patzkowsky, and Mike DiMarco. Dr. Sambhudas Chaudhuri provided helpful suggestions concerning analytical procedures and techniques.

GEOCHEMICAL INVESTIGATION
OF ROSITA HILLS VOLCANIC COMPLEX,
CUSTER COUNTY, COLORADO

by

Joseph Smalley

B.S., Wright State University, 1977

AN ABSTRACT OF

A MASTER'S THESIS

submitted in partial fulfillment of the
requirements for the degree

MASTER OF SCIENCE

Department of Geology
KANSAS STATE UNIVERSITY
Manhattan, Kansas

1981

The composition of Oligocene-Miocene volcanic rocks within the Rosita Hills volcanic complex in southern Colorado is primarily intermediate to rhyolitic. The rock types are characterized chemically by high alkali content (K_2O concentrations ranging from 3.5 to 8.0 percent) and by rare earth element (REE) concentrations that are significantly enriched and fractionated compared to typical basalt and peridotite.

Compositions of the various rock types form apparent trends on most major-element variation diagrams. This, together with similarities in phenocryst mineralogy, suggests that the different rock types exposed in the district might represent various stages of differentiation by fractional crystallization of a common parent magma. However, fractional crystallization modeling using partition coefficients from published sources suggests that simple fractionation of a common parent magma is an improbable explanation for the diversity of the suite. The variation in composition among the rock types probably reflects differences in conditions of melting of a common source rock.

Certain pairs of magma types within the suite, however, bear evidence of a common parent. Major-element data, trace-element data, field relations, and petrography are consistent with a model in which the latite (Tp) magma represents a differentiate of the trachyandesite (Tb). The available data are also consistent with the possibility that the syenodiorite (Tbs) could have evolved from the same liquid from which the lamprophyre (Tl) dikes were derived.

REE distributions of the suite are enriched in light REE (La, Ce) relative to heavy REE (Yb, Lu). This enrichment suggests that the magmas probably originated through partial melting of a garnet-bearing, high-pressure mineral assemblage such as eclogite or garnet peridotite. A likely source material for the intermediate to rhyolitic magma of the suite would be lower lithosphere eclogite. If such eclogite possessed concentrations of large-ion lithophile elements comparable to concentrations in typical continental basalt, then the eclogite would be capable of generating the fractionated REE distributions of the suite. Initial $^{87}\text{Sr}/^{86}\text{Sr}$ ratios of the intermediate and rhyolitic rock types of the suite range from 0.7057 to 0.7074, somewhat higher than would be expected in direct partial melting products of upper mantle garnet peridotite. The ratios are consistent, however, with partial melting of a lower lithospheric eclogite that itself may represent an ancient partial melting derivative of the mantle.

The lamprophyre (Tl) and syenodiorite (Tbs) require a more mafic source material and may be products of partial melting of garnet peridotite. Trace-element concentrations require either that the degree of melting in such a process be small (less than 10 percent) or that some other process, such as interaction with fluids, greatly altered the REE concentrations in these magma types.